CANADA

CROFILMED
BY
AL MICROFILM UNIT
LIC ARCHIVES
OF
CANADA
TTAWA, ONTARIO

MICROFILMÉ
PAR LE
SERVICE CENTRAL DU MICROFILM
ARCHIVES PUBLIQUES
DU
CANADA
OTTAWA, ONTARIO

- 20- 1971 DATE

REDUCTION 15x

Hébert OPERATOR
OPERATEUR

EXPOSURE
EXPOSITION 32

56)

ABSTRACT

A new class of improved reverse osmosis membranes, for casting solutions containing cellulose acetate, acetone and formamide, was developed based on the approach investigated earlier for aqueous magnesium-perchlorate-based membranes. The effects of casting solution composition and evaporation period on the performance of resulting porous cellulose acetate membranes have been studied, and the results, discussed in terms of casting solution structure, solvent evaporation rate during film formation and the film shrinkage temperature profile. The development of Batch 400 type porous cellulose acetate membranes is reported. Their productivities at 90% level of solute separation and feed flow conditions corresponding to a mass transfer coefficient of 45×10^{-4} cm/sec are approximately 22 gallons/day/sq. ft. at 250 psig and using 3500 ppm of NaCl in the feed and approximately 53.5 gallons/day/sq. ft. at 600 psig using 5000 ppm of NaCl in the feed.

ACKNOWLEDGMENT

The author is extremely grateful to Dr. S. Sourirajan for his indispensable guidance and direction in this project, and also to Dr. B. Kunst for his understanding and precious discussions. She wishes to thank Dr. B. C.-Y. Lu for his valuable assistance in discussions and for giving her the opportunity to work at the National Research Council. The author extends her gratitude to Dr. I. E. Puddington and Mr. W. S. Peterson for granting permission to carry out research studies at the National Research Council, and to Mr. L. Pageau and Mr. A. G. Baxter for their patience and valuable technical instructions.

LIST OF TABLES

LIST OF FIGURES (CONT'D) PAGE

NOMENCLATURE

A:	pure water permeability constant, $\frac{\text{g-mol } H_2O}{\text{cm}^2 \text{ sec atm}}$
a_W:	activity of water in aqueous solution
B:	evaporation rate value, grams $(\text{cm}^2)^{-1}$ min^{-1}
c:	molar density of solution, g-mol per cc.
c_1, c_2, c_3:	molar density of feed solution, concentrated boundary solution, and the product solution, respectively, g-mol per cc.
c_M:	molar density of solution in the membrane phase, g-mol per cc.
c_{M2}, c_{M3}:	molar density of solution in the membrane phase in equilibrium with c_2 and c_3, respectively, g-mol per cc.
D_{AB}:	diffusivity of solute in water, cm^2 per sec.
D_{AM}:	diffusivity of solute in membrane phase, cm^2 per sec.
$(D_{AM}/k\delta)$:	solute transport parameter, cm per sec.
f:	fraction solute separation
K:	proportionality constant defined by Equation 10.
k:	mass transfer coefficient on the high pressure side of membrane, cm per sec.
l:	thickness of the concentrated boundary solution
M_B:	molecular weight of water

Greek Letters

δ : effective thickness of membrane, cm.

ζ : normal distance towards membrane measured from edge of the concentrated boundary solution, cm.

π : osmotic pressure of solution, atm.

$\pi(X_A)$: osmotic pressure of solution corresponding to mole fraction X_A of solute, atm.

ϕ : osmotic coefficient

LITERATURE SURVEY

The reverse osmosis process is a general and widely applicable technique for the separation, concentration, or fractionation of inorganic or organic substances in aqueous or nonaqueous solutions in the liquid or the gaseous phase. The technique consists in letting the fluid mixture flow, under pressure, through an appropriate porous membrane, and withdrawing the membrane permeated product generally at atmospheric pressure and surrounding temperature; the product is enriched in one or more constituents of the mixture, leaving a concentrated solution on the upstream side of the membrane. No heating of the membrane and no phase change in product recovery are involved.

This process is a new development in the field of solute-solvent separation. Its most significant current application is in the field of water treatment, in general, and saline water conversion, in particular, for which porous cellulose acetate membranes have been found appropriate.

1. "Osmosis" and "Reverse Osmosis"

The term "Osmosis" is familiarly used to describe the spontaneous flow of pure water into an aqueous solution, or from a less to a more concentrated aqueous solution, when separated by a suitable membrane. In order to obtain potable water from saline water in a similar process, the direction of flow of the pure water must be reversed, i.e. pure water

must flow from a more to a less concentrated solution. Consequently the latter process has been conveniently termed "Reverse Osmosis". This term has now gained such wide popular usage that it seems necessary to point out that the process is not restricted to the passage of water from aqueous solutions, and that it is not restricted to 100 per cent solute separation, and that neither "osmosis" nor "reverse osmosis" is an explanation of the mechanism of the process involved, and hence it is misleading to explain "reverse osmosis" as the reverse of "osmosis". Under isothermal conditions, in both "osmosis" and "reverse osmosis", the preferential transport of material through the membrane is always in the direction of lower chemical potential. This is a thermodynamic requirement, and it does not, and cannot, specify which component, if any, of a solution will be preferentially transported through a given membrane, and the mechanism by which such transport takes place. In the literature, the "osmosis" process is always associated with the existence of a "semipermeable" membrane; the cause of such semipermeability however continues to remain obscure. Hence it must be understood that the mechanism of both "osmosis" and "reverse osmosis" is still an open question, and the distinction between the two terms is entirely one of arbitrary convention and popular usage.

Based on the transport of water from aqueous solutions due to the chemical potential gradient, a variety of membrane separation processes can be developed as indicated in Figure 1. The discussion in this work is restricted to the transport

FIGURE 1

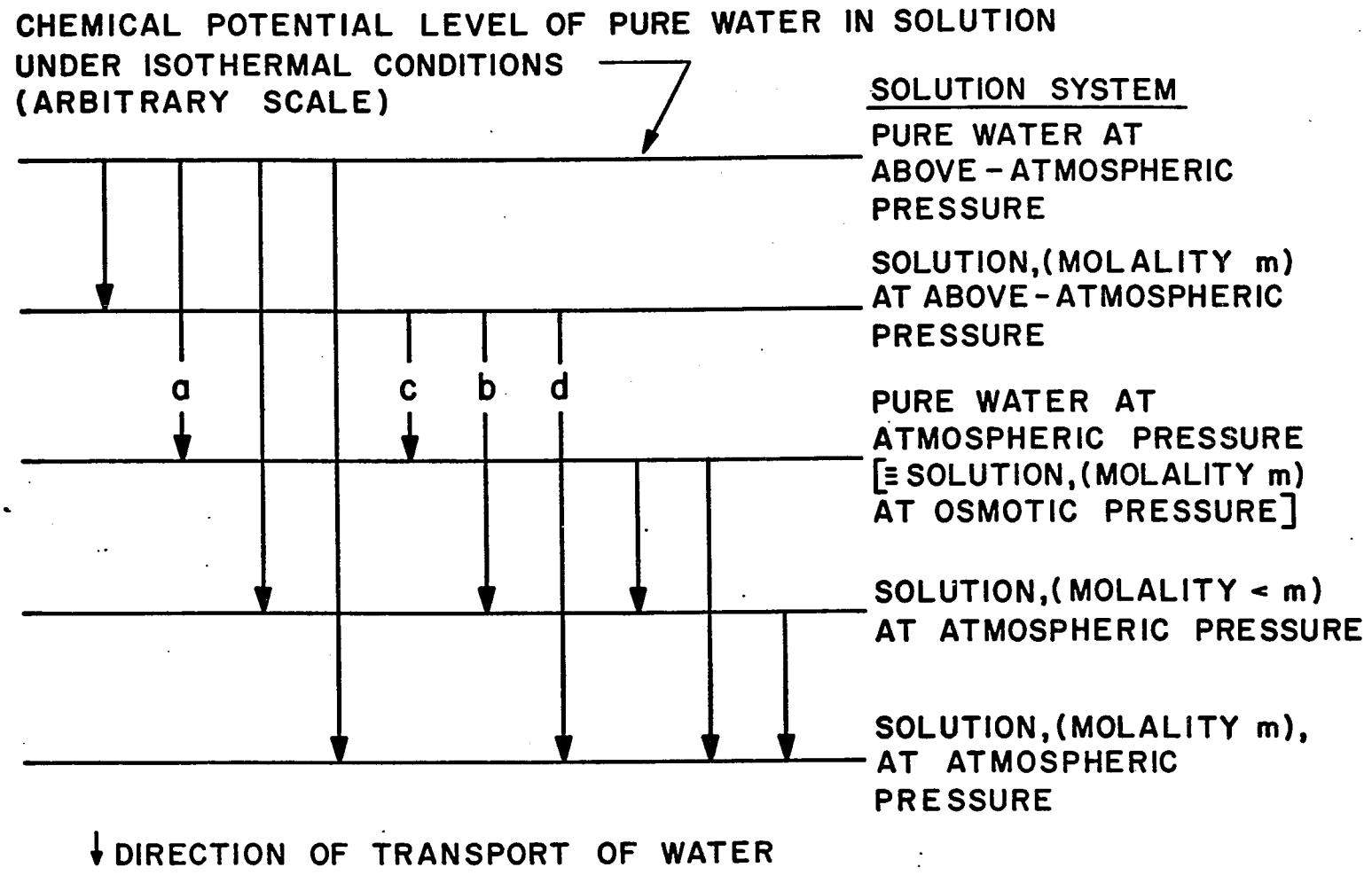
CHEMICAL POTENTIAL LEVEL OF PURE WATER IN SOLUTION UNDER ISOTHERMAL CONDITIONS (ARBITRARY SCALE)
SOLUTION SYSTEM
PURE WATER AT ABOVE-ATMOSPHERIC PRESSURE
SOLUTION,(MOLALITY m) AT ABOVE-ATMOSPHERIC PRESSURE
a
c
b
d
PURE WATER AT ATMOSPHERIC PRESSURE [≡SOLUTION,(MOLALITY m) AT OSMOTIC PRESSURE]
SOLUTION,(MOLALITY < m) AT ATMOSPHERIC PRESSURE
SOLUTION,(MOLALITY m), AT ATMOSPHERIC PRESSURE
DIRECTION OF TRANSPORT OF WATER

A solution-diffusion mechanism is favored by Lonsdale et al (36-39,44), whose transport equations are apparently limited to their concept of "perfect" membranes, which are presumably those which have a completely nonporous surface structure. Banks and Sharples (1-3),also consider that the mechanism of reverse osmosis is one of diffusive flow through the pore-free layer on the membrane surface. According to Michaels et al (42), water transport in reverse osmosis is by molecular diffusion through the polymer matrix, and solute transport is by parallel mechanisms involving sorption, activated diffusion, and hydrodynamic flow. According to Sherwood et al (46), water and solute cross the membrane by parallel processes of diffusion and pore flow. The reverse osmosis process has also been interpreted in terms of non-equilibrium thermodynamics by several workers.

3. Preferential Sorption-Capillary Flow Mechanism

This has been discussed in detail by Sourirajan (47). According to this mechanism, reverse osmosis separation is the combined result of an interfacial phenomenon and fluid transport under pressure through capillary pores, and the appropriate membrane is a porous medium at all levels of solute separation. That the membrane surface is porous and heterogeneous, and that the transport of both the preferentially sorbed water and the aqueous solution is through the capillary pores in the membrane surface, are concepts fundamental to this approach.

FIGURE 2

SCHEMATIC REPRESENTATION OF PREFERENTIAL SORPTION-CAPILLARY FLOW MECHANISM. (47)

FIGURE 2

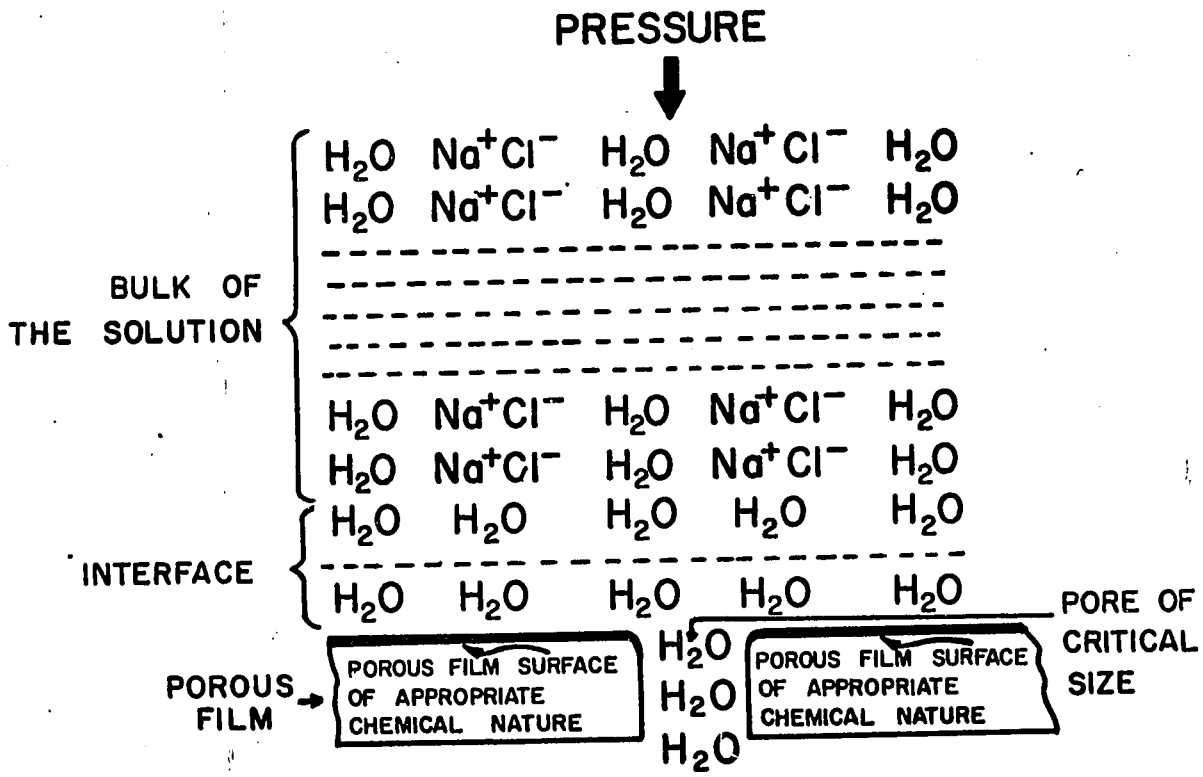
PRESSURE
BULK OF THE SOLUTION
INTERFACE
POROUS FILM
POROUS FILM SURFACE OF APPROPRIATE CHEMICAL NATURE
POROUS FILM SURFACE OF APPROPRIATE CHEMICAL NATURE
PORE OF CRITICAL SIZE

FIGURE 3

CRITICAL PORE DIAMETER FOR MAXIMUM SEPARATION AND PERMEABILITY. (47)

FIGURE 3

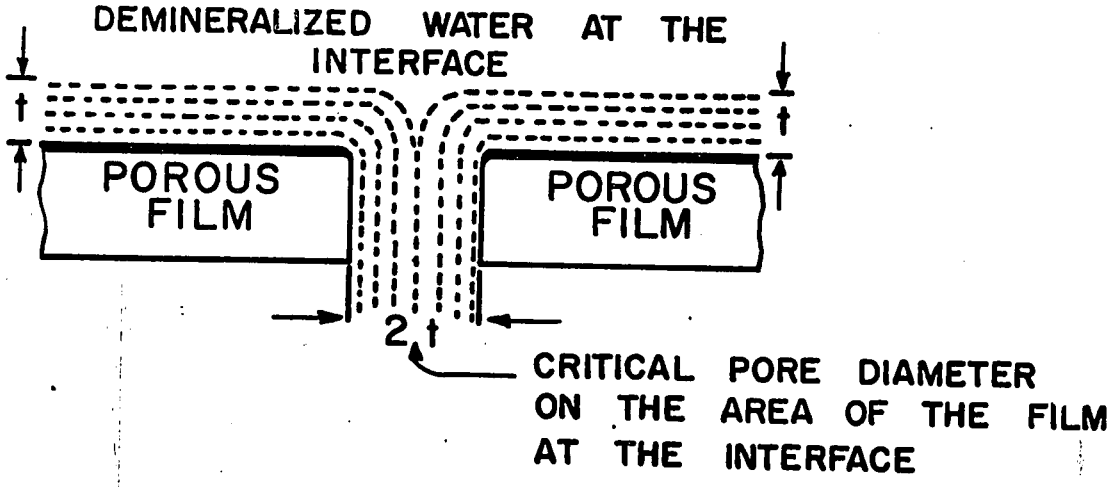
DEMINERALIZED WATER AT THE INTERFACE
t
t
POROUS FILM
POROUS FILM
2t
CRITICAL PORE DIAMETER ON THE AREA OF THE FILM AT THE INTERFACE

degree of solute separation is possible, depending on the porous structure of the membrane and other operating conditions. These two characteristics are borne out experimentally.

From an industrial standpoint, the application of the reverse osmosis techniques for a given separation problem involves essentially the problem of choosing the appropriate chemical nature of the film surface and developing methods for making films containing the largest number of pores of the required size on the area of the film at the interface. This approach formed the basis of the successful development of the Loeb-Sourirajan-type porous cellulose acetate membranes for saline water conversion and similar applications.

4. Microporous Nature of Surface Layer in Reverse Osmosis Membrane

The practical consequence of the microporous nature of the surface layer in the reverse osmosis membrane constitutes the basis of the work of Kopeček and Sourirajan (19-22). This basis is also supported by the theoretical work of Glueckauf (6), and Meares (41), and the following three important experimental observations with respect to the Loeb-Sourirajan type porous cellulose acetate membranes.

A) Shrinkage Temperature vs Solute Separation and Product Rate

Using a 0.5 M [$NaCl-H_2O$] feed solution, at an operating pressure of 1,500 psig, a membrane without any prior thermal

treatment gives very high product rate (>300 gal/day/sq. ft.) and very little solute separation. These data indicate that the surface of a typical untreated membrane is quite porous.

Solute separation can be progressively increased by heating the membrane under water for short periods of time as stated earlier. The effect of temperature treatment then is to shrink the size of the pores on the membrane surface. When the shrinkage temperature is increased, the size of the pores on the membrane surface becomes smaller; consequently solute separation increases, and product rate decreases. This is illustrated in Figure 4 which gives the results obtained with several films shrunk at different temperatures.

On progressively increasing the shrinkage temperature, solute separation can be increased to levels >98 or 99%, and still good product rates can be obtained. There is nothing to indicate however that at this stage the pores on the membrane surface have been closed, and the membrane surface has become essentially nonporous; on the contrary, the following data indicate that the membrane surface still remains microporous.

On increasing the shrinkage temperature still further after reaching the stage of 98 to ~100% solute separation, the product rate does not remain constant (as we would expect if the membrane surface is nonporous), but it is reduced still further indicating that the size of the pores on the membrane

FIGURE 4

BEHAVIOUR OF SOME POROUS CELLULOSE-ACETATE MEMBRANES AT DIFFERENT SHRINKAGE TEMPERATURES. (47)

surface are getting still further reduced. This thermal pretreatment procedure can be carried far enough to close practically all the pores on the membrane surface and reduce the product rate to negligible levels. This is illustrated in Figure 5 with respect to the CA-NRC-18 type films.

The above shrinkage temperature-product rate profile obtained under conditions of high solute separation (near 100%) cannot be attributed to any steep increase in effective film thickness brought about by high shrinkage-temperature, for at least two reasons. First, the shrinkage temperature-product rate profile is different for films cast under different conditions; whatever be the above profile, the behaviour of the films is similar. Secondly, any steep increase in thickness of the surface layer at any temperature should also result in an abrupt change in the mechanical properties of the film at that temperature; Keilin et al (7-10) found no abrupt changes in the mechanical properties of the porous cellulose acetate membranes in a wide range of temperature.

The above observations indicate that even at the near 100% level of solute separation, the Loeb-Sourirajan type porous cellulose acetate membranes have microporous surface structure.

B) Effect of Temperature on Pure Water Permeability Constant, A

The pure water permeability, [PWP], data (expressed as A in g.mole H_2O/sq. cm. sec. atm.) for a set of four different

FIGURE 5

PERFORMANCE OF B-18 TYPE MEMBRANES. (47)

CA-NRC-18 type films were obtained in the operating temperature range 6 to 36°C. The films were shrunk at different temperatures and hence capable of giving different levels of solute separation. With a 0.5 M [NaCl-H_2O] feed solution at 1,500 psig, the films 23, 24, 25, and 26 gave solute separations of 28.2, 49.0, 68.9, and 97.1% respectively; the pure water permeability constant A increased with increase in operating temperature, and A multiplied by the viscosity of water at the operating temperature remained constant for all the films tested as illustrated in Figure 6. These results indicate that fluid flow through each of the above films is essentially viscous, and the mechanism of fluid transport is the same for all the films tested, and hence all the above films have microporous surface structures, and they differ essentially in the magnitude of the average size of their surface pores.

C) Pure Water Permeability Constant, A, vs Solute Transport Parameter, ($D_{AM}/K\delta$)

The values of A (which expresses pure water permeability), and ($D_{AM}/K\delta$) for NaCl (which is analogous to a mass transfer coefficient for solute transport) for a number of CA-NRC-18 type films were determined by the Kimura-Sourirajan analysis. An increase in the value of A corresponds to an increase in the average pore size on the membrane surface. The films chosen covered a wide range of solute separation; for example, with respect to a 0.5 M feed solution, films G1 and 12 gave

FIGURE 6

EFFECT OF OPERATING TEMPERATURE ON THE PURE WATER PERMEABILITY CONSTANT A MULTIPLIED BY THE VISCOSITY OF WATER, μ_W, AT THE OPERATING TEMPERATURE. (47)

FIGURE 6

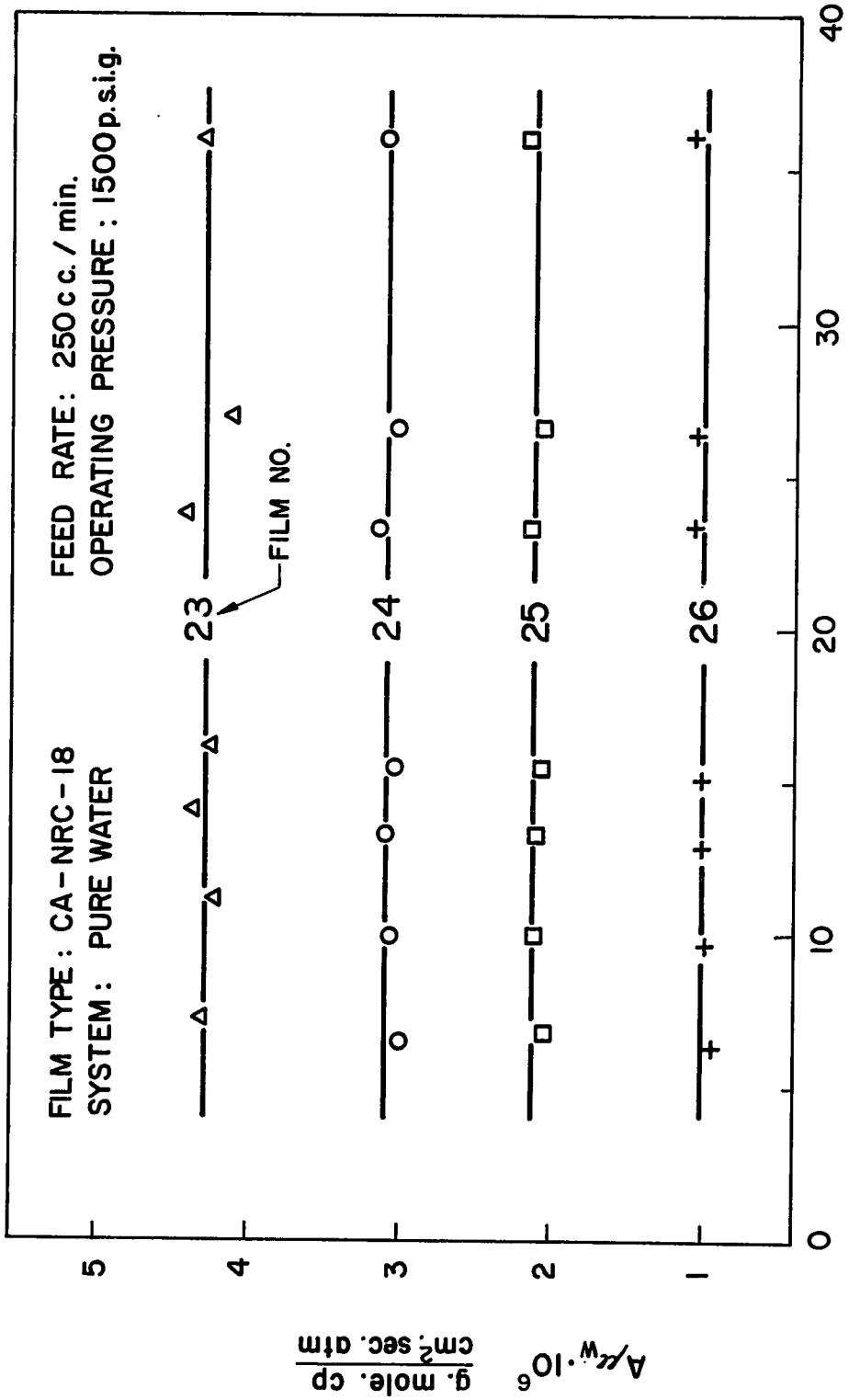
FILM TYPE : CA-NRC-18
SYSTEM : PURE WATER
FEED RATE : 250 c.c. / min.
OPERATING PRESSURE : 1500 p.s.i.g.
FILM NO.
23
24
25
26
5
4
3
2
1
0
10
20
30
40
TEMPERATURE °C.
$A/\ell_w \cdot 10^6$ g. mole. cp / cm². sec. atm

98.9 and 18.7% solute separation respectively; the other films gave intermediate levels of solute separation. A log-log plot of A vs $(D_{AM}/K\delta)$ is shown in Figure 7. The absence of any abrupt discontinuity in the A vs $(D_{AM}/K\delta)$ correlation shows that the mechanism of solute and solvent transport in film G1 is no different from that in film 12, which again means that all the above films had microporous surface structures, and they differed only in the magnitude of the average size of their surface pores.

5. Method for Improving the Performance of Porous Cellulose Acetate Membranes

The preferential sorption-capillary flow mechanism offers several approaches to the problem of improving the performance of porous cellulose acetate membranes (i.e. increasing their product rates without decreasing solute separation): (i) the effective thickness of the membrane (especially the thickness of the microporous surface layer controlling solute separation) may be reduced; (ii) the absolute number of pores of appropriate size on the microporous surface layer may be increased; (iii) the rigidity of the overall porous structure of the membrane may be altered so that membrane compaction is less during continuous operation under pressure, and/or (iv) the number, pore size and pore size distribution on the microporous surface layer of a given membrane may be altered such that increased permeability results without decreasing solute separation.

FIGURE 7

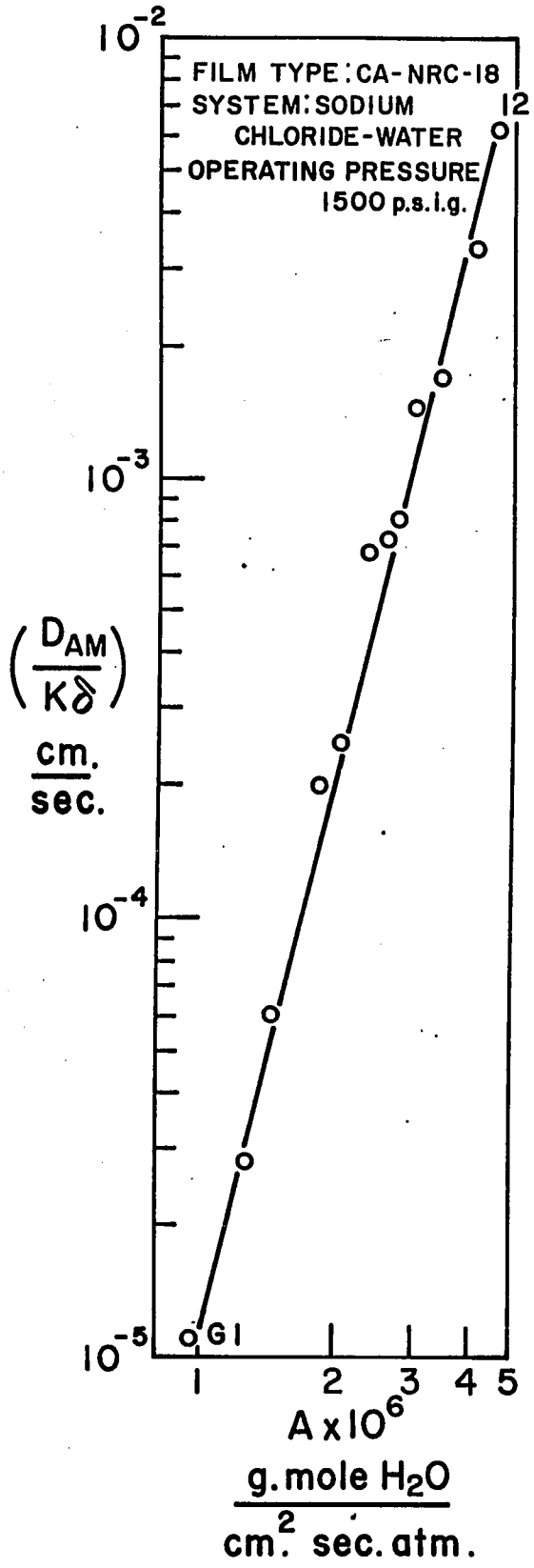
FILM TYPE: CA-NRC-18
SYSTEM: SODIUM CHLORIDE-WATER
OPERATING PRESSURE 1500 p.s.i.g.
12
G1
10^{-2}
10^{-3}
10^{-4}
10^{-5}
$\left(\frac{D_{AM}}{K\delta}\right)$ cm./sec.
1 2 3 4 5
A x 10^6
g. mole H_2O / cm^2 sec. atm.

THEORETICAL CONSIDERATIONS

1. Transport Through Reverse Osmosis Membranes

The following discussion is restricted to isothermal reverse osmosis separation process involving binary aqueous solution systems and Loeb-Sourirajan-type porous cellulose acetate membranes having a preferential sorption for water from the aqueous solution under consideration. Unless otherwise stated, all data presented in this work are for 25°C.

A) Osmotic pressure. The osmotic pressure, π, of a solution is given by the relationships of:

$$\pi = \frac{-RT}{\bar{V}_w} \ln a_w \qquad (1)$$

$$= \frac{\Sigma i \; RT \; M_B}{1000 \; \bar{V}_w} \; m\phi \qquad (2)$$

The values of π for many solutions can be calculated from the activity (a_w) or the osmotic coefficient (ϕ) data available in the literature (45).

B) Concentration polarization. The existence and the continuous withdrawal of the preferentially sorbed interfacial layer along with the bulk feed solution through the porous membrane give rise to a product solution less concentrated than the feed solution and a more concentrated boundary solution between the interfacial region on the membrane surface and the bulk feed solution. Consequently, under steady-state operating conditions, there arises a concentration gradient between the

boundary solution and the bulk feed solution (Figure 8). This concentration gradient, called "concentration polarization", has important effects on the performance of reverse osmosis systems.

With respect to a given membrane-solution system, the magnitude of the interfacial region is a function of the concentration of the boundary solution, and the effective driving pressure (ΔP) for fluid flow through the membrane is the operating pressure, P, minus the difference between the osmotic pressure of the concentrated boundary solution, $\pi(X_{A2})$, and that of the membrane permeated product solution, $\pi(X_{A3})$.

C) Maximum separation. Under the reverse osmosis operating conditions,

$$\Delta P = P - \Delta\pi \qquad (3)$$

and

$$\Delta\pi = \pi(X_{A2}) - \pi(X_{A3}) \qquad (4)$$

For the limiting case, when the mass transfer coefficient on the high pressure side of the membrane tends to infinity, $\pi(X_{A2})$ approaches the osmotic pressure of the feed solution, $\pi(X_{A1})$.

When P is equal to or less than $\pi(X_{A2})$, Equation 3 also gives the maximum solute separation possible in this process whatever membrane is used, under which condition

$$\Delta\pi = P, \text{ and } \Delta P = 0 \qquad (5)$$

If we use Equation 5 and let $\pi(X_{A2}) = \pi(X_{A1})$, Figure 9 gives the plot of the maximum solute separation possible (f max)

FIGURE 8

REVERSE OSMOSIS PROCESS UNDER STEADY-STATE CONDITIONS. (47)

FIGURE 8

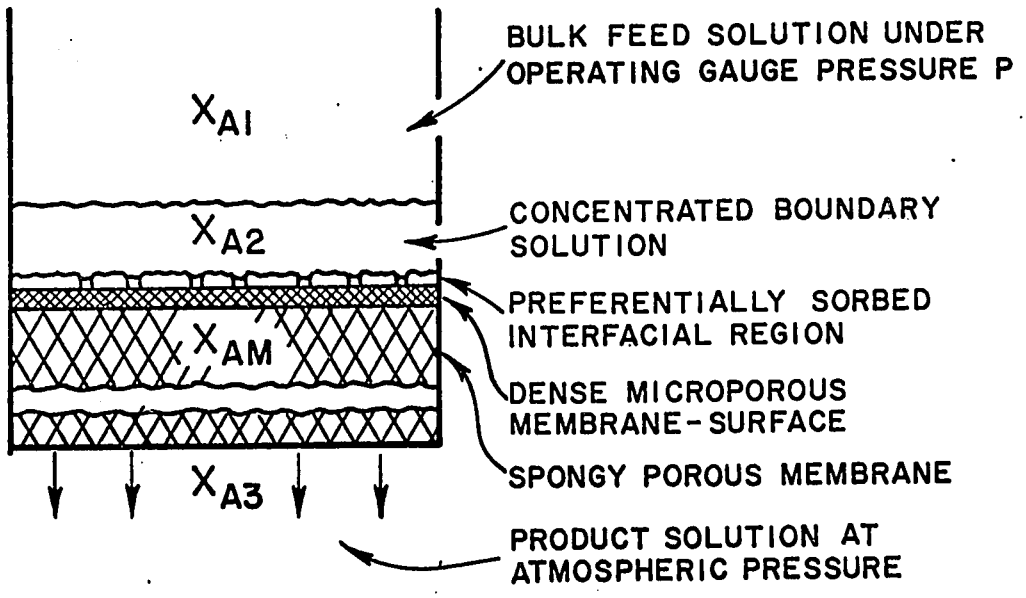
BULK FEED SOLUTION UNDER
OPERATING GAUGE PRESSURE P
X_{A1}
CONCENTRATED BOUNDARY
SOLUTION
X_{A2}
PREFERENTIALLY SORBED
INTERFACIAL REGION
X_{AM}
DENSE MICROPOROUS
MEMBRANE-SURFACE
SPONGY POROUS MEMBRANE
X_{A3}
PRODUCT SOLUTION AT
ATMOSPHERIC PRESSURE

FIGURE 9

MAXIMUM POSSIBLE SOLUTE SEPARATIONS FOR THE SYSTEM SODIUM CHLORIDE-WATER IN THE REVERSE OSMOSIS PROCESS AT DIFFERENT OPERATING PRESSURES AND FEED CONCENTRATIONS. (47)

for the system sodium chloride-water at different operating pressures and feed concentrations. Figure 9 illustrates the thermodynamic significance of osmotic pressure as applied to this separation process.

When P is equal to or less than $\pi(X_{Al})$, the values of f max given in Figure 9 correspond to the condition that the product rate is zero; when P is greater than $\pi(X_{Al})$, there is no thermodynamic limitation to the extent of solute separation and product rate obtainable in this process.

While Equation 3 is true whatever the value of the osmotic pressure of the feed solution, it says nothing about the separation characteristics of any membrane. In other words, the actual performance of any particular membrane with respect to a given solution system depends, not only on the osmotic pressure of the feed solution, but also on the physical and chemical nature of the membrane.

2. Kimura-Sourirajan Analysis of Reverse Osmosis Experimental Data

This analysis (11-16) is applicable for the entire possible range of solute separations in the reverse osmosis process. In this analysis, PWP is directly proportional to the operating pressure, and the proportionality constant obtained is called the pure water permeability constant, A; the transport of solvent water N_B, through the membrane is proportional to the effective pressure where the proportionality constant is A; the transport

Equation 8 is applicable for systems where the kinematic viscosity of the product solution is not too different from that of pure water. This condition is reasonably satisfied in most cases of practical interest.

There is no easy method to determine X_{A2} experimentally. Hence, one cannot be certain that X_{A2} calculated from Equation 8 is the true value of X_{A2}. This uncertainty, however, is no limitation in the Kimura-Sourirajan analysis so long as the correlation between the solute transport parameter (discussed below) and X_{A2} can be specified on the basis of Equation 8.

C) Transport of solute (N_A) through membrane phase:

$$N_A = \frac{D_{AM}}{\delta} (c_{M2} X_{AM2} - c_{M3} X_{AM3}) \qquad (9)$$

None of the quantities on the right side of Equation 9 are known, and the dividing line in the membrane phase between the regions corresponding to X_{AM2} and X_{AM3} is only conceptual. Equation 9 can be transformed into one containing measurable quantities and a group of unknown quantities by assuming a simple linear relationship between X_A (concentration in the solution phase) and X_{AM} (concentration in the membrane phase). Thus let

$$c X_A = K c_M X_{AM} \qquad (10)$$

so that

$$c_2 X_{A2} = K c_{M2} X_{AM2} \qquad (11)$$

and

$$c_3 X_{A3} = K c_{M3} X_{AM3} \qquad (12)$$

the surface of the membrane. That this is true has been shown experimentally, as illustrated in Figure 10, for the system sodium chloride-water.

D) Mass transfer on the high-pressure side of the membrane:

The solute transfer from the concentrated boundary solution may be represented by the relation (12)

$$N_A = X_A (N_A + N_B) - D_{AB} c_1 \frac{dX_A}{d\zeta} \qquad (17)$$

or, by use of Equation 14,

$$\frac{dX_A}{d\zeta} - \frac{(N_A + N_B)}{c_1 D_{AB}} X_A = - \frac{(N_A + N_B)}{c_1 D_{AB}} X_{A3} \qquad (18)$$

where ζ represents normal distance toward membrane measured from edge of the concentrated boundary solution. Equation 17, expressing N_A as the resultant of two vector quantities, is a form of Fick's first law of diffusion. Under steady-state conditions, $(N_A + N_B)$ is the total flux through the membrane, and Equation 17 is applicable at any point in the reverse osmosis system. The boundary conditions for Equation 18 are when

$$\zeta = 0, \quad X_A = X_{A1} \qquad (19)$$

and when

$$\zeta = 1, \quad X_A = X_{A2} \qquad (20)$$

Solving Equation 18:

$$X_{A2} = X_{A3} + (X_{A1} - X_{A3}) \exp. \left[\frac{(N_A + N_B)}{c_1} \frac{1}{D_{AB}} \right] \qquad (21)$$

or

FIGURE 10

CONCENTRATION OF SOLUTE IN THE BOUNDARY SOLUTION VS THAT IN THE PRODUCT SOLUTION FOR THE SYSTEM SODIUM CHLORIDE-WATER. (47)

FIGURE 10

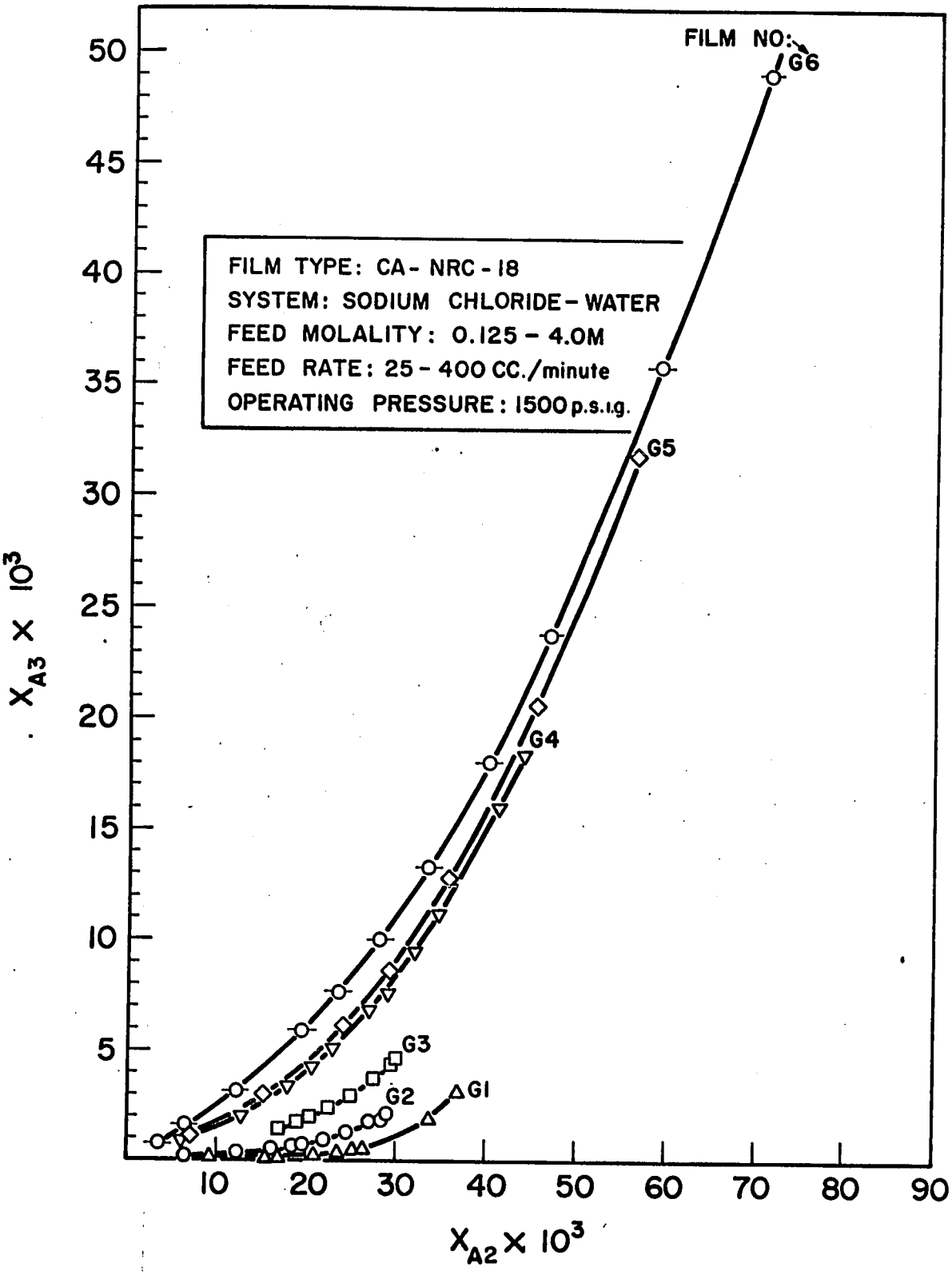
FILM NO:
G6
G5
G4
G3
G2
G1
FILM TYPE: CA - NRC - 18
SYSTEM: SODIUM CHLORIDE - WATER
FEED MOLALITY: 0.125 - 4.0M
FEED RATE: 25 - 400 CC./minute
OPERATING PRESSURE: 1500 p.s.i.g.
$X_{A3} \times 10^3$
$X_{A2} \times 10^3$
50
45
40
35
30
25
20
15
10
5
10
20
30
40
50
60
70
80
90

$$\ln \left[\frac{X_{A2} - X_{A3}}{X_{A1} - X_{A3}} \right] = \frac{(N_A + (N_B)}{c_1} \frac{1}{D_{AB}} \qquad (22)$$

Defining the mass transfer coefficient, k, on the high-pressure side of the membrane in the conventional manner of the film theory:

$$k = \frac{D_{AB}}{l} \qquad (23)$$

and by use of Equations 14 and 15

$$\ln \left[\frac{X_{A2} - X_{A3}}{X_{A1} - X_{A3}} \right] = \frac{N_B}{k\, c_1\, (1 - X_{A3})} \qquad (24)$$

or

$$N_B = k\, c_1\, (1 - X_{A3}) \ln \left[\frac{X_{A2} - X_{A3}}{X_{A1} - X_{A3}} \right] \qquad (25)$$

From the foregoing analysis, Equations 6, 8, 16, and 25 emerge as a set of basic equations describing the solute and solvent transport in a reverse osmosis process involving binary aqueous solutions and membranes having a preferential sorption for water from such aqueous solutions. For many solutions of practical interest, such as sodium-chloride-water, the molar density (c) may be assumed constant - i.e.,

$$c = c_1 = c_2 = c_3$$

so that the basic transport equations in reverse osmosis may be summarized as follows:

$$A = \frac{PWP}{M_B \times S \times 3600 \times P} \qquad (6)$$

TABLE I

Film Casting Details for Magnesium Perchlorate-Based Membranes (24)

Film Casting Details	Batch 25	Batch 18	Batch 301	Batch 316
Casting solution composition, wt.%				
Cellulose acetate (acetyl content 39.8%)	22.2	17	17	17
Acetone	66.7	68	68	69.2
Magnesium perchlorate	1.1	1.5	1.5	1.45
Water	10.0	13.5	13.5	12.35
Formamide	----	----	----	----
Casting solution temperature, ^{o}C	-5^{o} to $-10^{o}C$	-10	0	0
Temp. of casting atmosphere, ^{o}C	-5^{o} to $-10^{o}C$	-10	23-25	24
Casting atmosphere	ambient air	ambient air	ambient air in contact with aqueous solution of 30 wt.% acetone	ambient air in contact with aqueous solution of 30 wt.% acetone
Solvent evaporation time, min.	4	4	2	6
Duration of film-setting in ice-cold water, hour	~1	~1	~1	>1
Nominal film thickness, inch	0.004	0.004	0.004	0.004

and Sourirajan, (23) the above two temperatures constitute two separate variables.

The emergence of Batch 301 type membranes is the result of a new approach to the general problem of developing more productive reverse osmosis membranes. In this approach, the state or the structure of the casting solution and the rate of solvent evaporation during film formation together constitute an important interconnected variable governing the ultimate porous structure, and hence the performance of the resulting membranes in reverse osmosis.

The distinguishing feature of the new approach to reverse osmosis membrane research described above lies in the analysis of the usual film casting variables in terms of correlating membrane performance data with the casting solution structure, solvent evaporation rate during film formation, and the shrinkage temperature profile. The above approach forms the basis of this work which extends the earlier investigations on the cellulose acetate-acetone-aqueous magnesium perchlorate casting solution system to the cellulose acetate-acetone-formamide casting solution system with particular reference to the effects of changes in the casting solution composition and in the nature and temperature of the casting atmosphere on the performance of the resulting membranes. This work has led to the development of Batch 400 type porous cellulose acetate membranes which give the same performance as Batch 316 type membranes (Fig. 11) for low pressure reverse osmosis desalination and other applications.

FIGURE 11

COMPARATIVE PERFORMANCE AND SHRINKAGE

PROFILE OF BATCH 400 MEMBRANES AT 250 PSIG

FIGURE 11

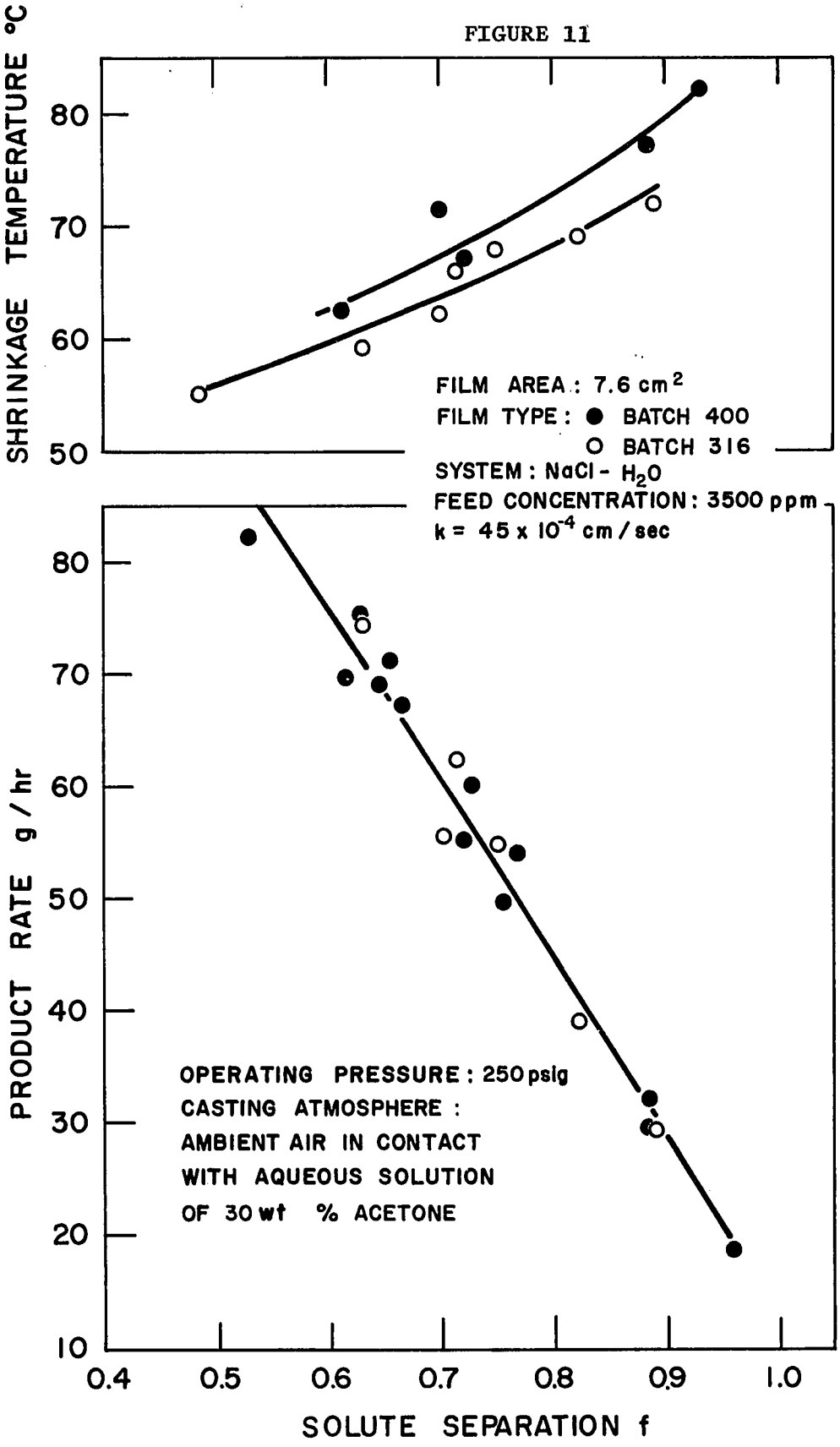
SHRINKAGE TEMPERATURE °C
80
70
60
50
FILM AREA : 7.6 cm²
FILM TYPE : ● BATCH 400
○ BATCH 316
SYSTEM : NaCl - H₂O
FEED CONCENTRATION : 3500 ppm
k = 45 x 10⁻⁴ cm / sec
PRODUCT RATE g / hr
80
70
60
50
40
30
20
10
OPERATING PRESSURE : 250 psig
CASTING ATMOSPHERE :
AMBIENT AIR IN CONTACT
WITH AQUEOUS SOLUTION
OF 30 wt % ACETONE
0.4
0.5
0.6
0.7
0.8
0.9
1.0
SOLUTE SEPARATION f

FIGURE 12

REVERSE OSMOSIS CELL. (47)

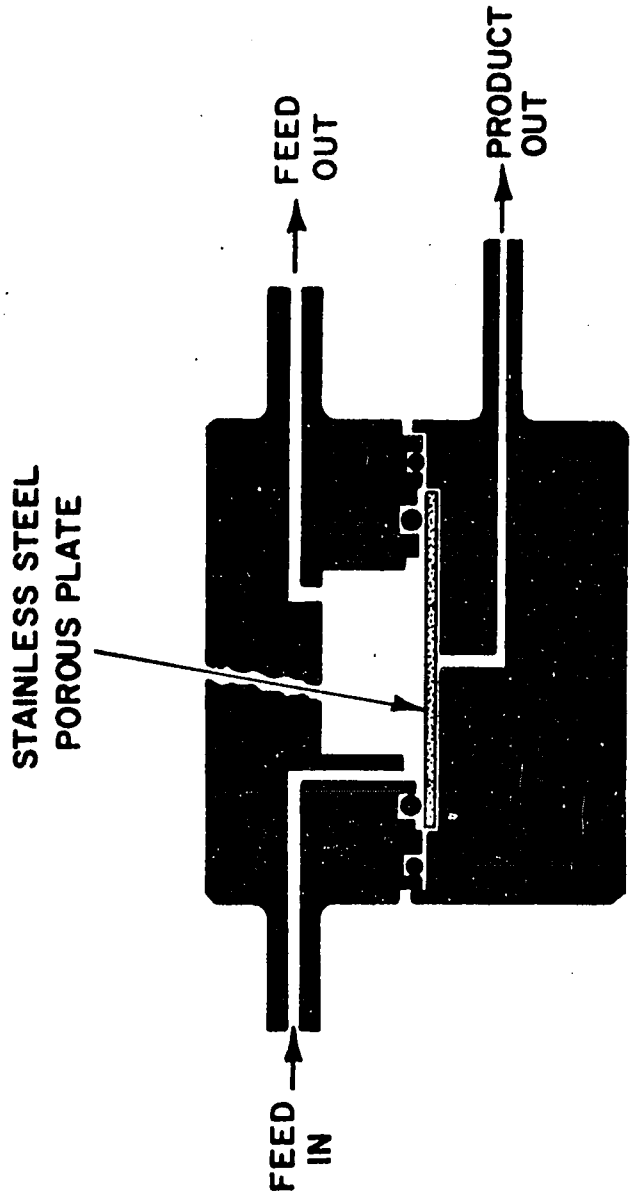

FIGURE 12

is shown in Figure 13. A positive displacement pump was used to pump the feed solution under pressure through the cell. All parts of the pump coming into contact with the feed liquid were made of stainless steel. The surge tank, a stainless steel high pressure cylinder (2-inches O.D. x 1 1/2-inches I.D. x 14 inches high), was used to minimize the pressure fluctuations in the cell. A porous stainless steel plate specified to have pores of average size equal to 5 microns was mounted between the pump and the cell to act as a filter for dust particles which might otherwise clog the pores on the membrane surface. Under the operating conditions the fluid pressure in the cell was indicated by a liquid sealed Ashcroft pressure gauge. The purge valve was used to drain the system whenever necessary. A stainless steel Grove pressure regulator was used to maintain a constant operating pressure in the cell. Nitrogen gas under pressure from commercial gas cylinders was used to load the dome of the Grove regulator. Monel metal high pressure tubings and HIP high pressure fittings made of 316 Stainless Steel were used throughout the system.

Six cells were used in series - (only one cell illustrated in Figure 13) - so that six different membranes could be tested at the same time. Samples of the feed solution entering each cell could be drawn separately, if necessary. Membranes shrunk at different temperatures were used to give different levels of solute separation at a given set of operating conditions. Unless

FIGURE 13

SCHEMATIC FLOW DIAGRAM OF APPARATUS. (47)

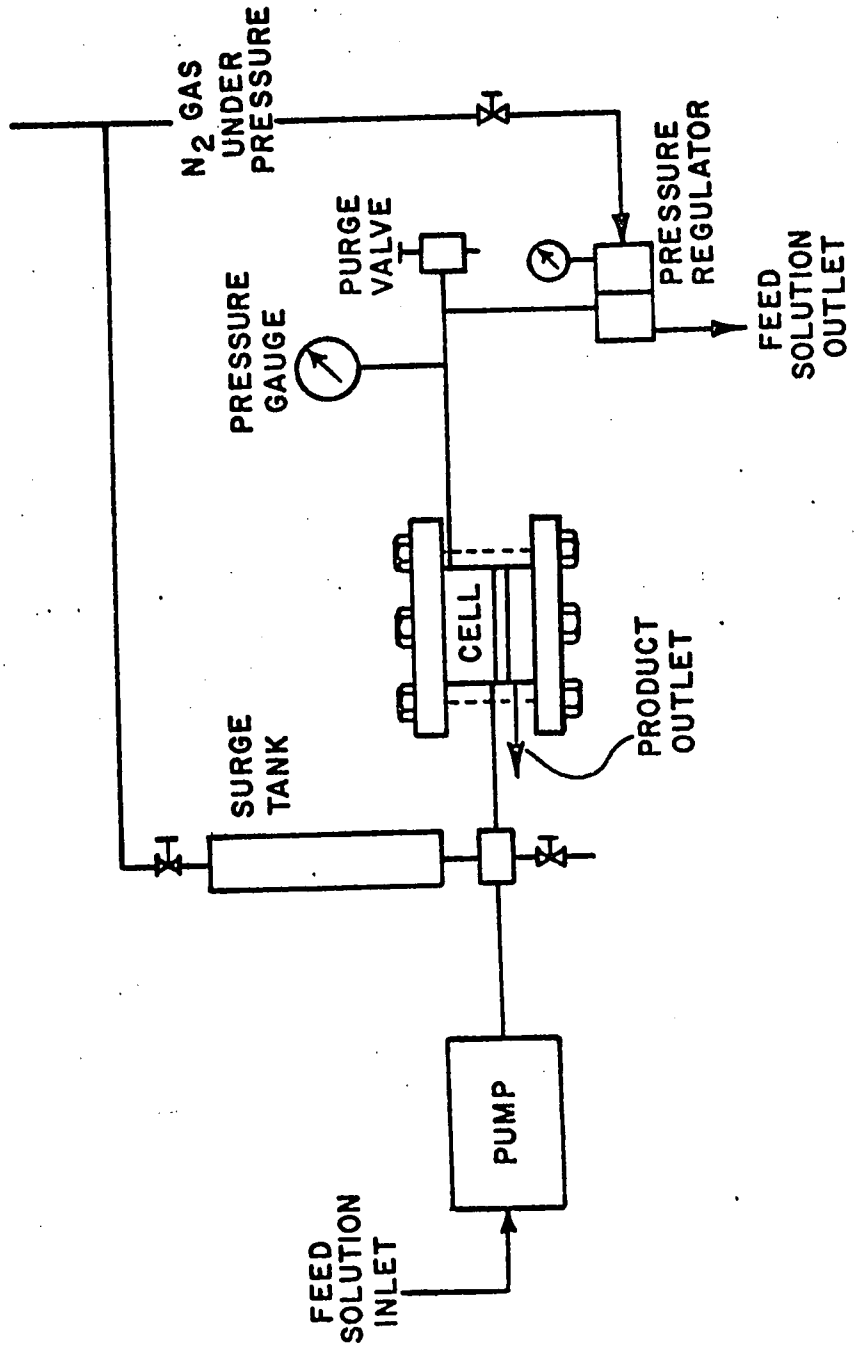
N_2 GAS UNDER PRESSURE
PURGE VALVE
PRESSURE REGULATOR
PRESSURE GAUGE
FEED SOLUTION OUTLET
CELL
PRODUCT OUTLET
SURGE TANK
PUMP
FEED SOLUTION INLET

FIGURE 13

otherwise stated, the experiments were of the short run type, each lasting for about 2 hours; they were carried out at the laboratory temperature; the effective area of the film used was 7.6 sq. cm., the reported product rates were those corrected to 25°C. using the relative viscosity and density data for pure water.

3. Membrane preparation procedure.

The preparation of reverse osmosis membrane consists of five main steps: 1) stirring and 2) casting of the casting solution, 3) shrinking and 4) pressurization of the membrane and 5) the reverse osmosis run itself. The film-casting solution contains cellulose acetate (acetyl content 39.8%, ASTM Visc. 3), acetone (reagent A.C.S.), and formamide and is stirred by a rotatory motor in a glass bottle for 24 hours. With the above solution, membranes are cast on flat glass plates either at laboratory or lower temperatures. After it is cast, part of the solvent is allowed to evaporate for a definite period from the surface of the membrane at the casting temperature. This is followed by immersing the membrane in ice cold water for at least 12 hours; during the immersion time, the film sets to a gel, from which the formamide and the solvent (acetone) are leached out, leaving a tough solid porous film on the flat surface, from which it can be removed easily. All details relating to the casting-solution composition, stirring, evaporation, and gelation steps are important in developing successful reverse osmosis membranes. These membranes are always stored at laboratory temperature, and under water since on drying in the air, their porous structure

generally changes irreversibly. Films cast in the above manner have a relatively dense microporous structure (pore size probably <50Å) on an extremely thin layer (about 10^{-5} in.) of the film surface which was exposed to the atmosphere during casting; this side of the film is called the "surface layer side", and the other side, the "back side". The remainder of the film material underneath this thin surface layer is a spongy porous mass containing, comparatively, very big pores ($\sim$ 4000Å). Consequently, the above films are said to have an asymmetric porous structure. It is the microporous structure of the dense surface layer which governs the level of solute separation, and hence is held in contact with the feed solution during reverse osmosis operation.

In the as-cast condition, the surface pores are generally too big to give any significant solute separation. But the membrane can be shrunk and the pore size reduced by simply keeping the film immersed in hot water in a controlled heat bath for about 10 min. Thus, by adjusting the shrinkage temperature, different porosities on the surface layer side of the membrane, capable of giving different levels of solute separation, can be obtained.

All membranes are then subjected to a pure water pressure of 300 psig for an hour before use in reverse osmosis experiments. The latter are of the short-run type, each lasting for about 2 hours; they are carried out at the laboratory temperature, using aqueous feed solutions containing 3500 ppm. of NaCl and a feed rate of 330 cc. per minute at the operating pressure of 250 psig.

The reported product rates are those corrected to 25°C using the relative viscosity and density data for pure water. In each experiment, the solute separation f, defined as

$$f = \frac{\text{solute concn. in feed (ppm)} - \text{solute concn. in product (ppm)}}{\text{solute concn. in feed (ppm)}}$$

the product rate, [PR], and the pure water permeability, [PWP], in grams per hour per 7.6 sq. cm. of effective film area were determined at the operating conditions. In all cases, the terms "product" and "product rate" refer to the membrane permeated solutions. The solute concentrations in feed and product solutions were determined by specific resistance measurements using a conductivity cell. The accuracy of the separation data is within 1% and that of [PR] and [PWP] data is within 3% in all cases. The average mass transfer coefficient on the high pressure side of the membrane under the experimental conditions was 45×10^{-4} cm. per second as calculated by the Kimura-Sourirajan analysis of the reverse osmosis experimental data.

4. Solvent evaporation rate measurements.

These were made by determining the change in weight of the polymer film cast on a small plate as a function of time. Small stainless steel plates (effective surface area 1.61 cm x 5.06 cm) grooved to different depths from 0.025 to 0.041 cm were used for film casting which was done by a hand-operated mechanical device (Figure 14) attached to the side door of an analytical balance. In this arrangement, the plate entered the closed space of the balance case simultaneously as the film was being formed on it

FIGURE 14

MECHANICAL DEVICE USED FOR EVAPORATION RATE MEASUREMENTS

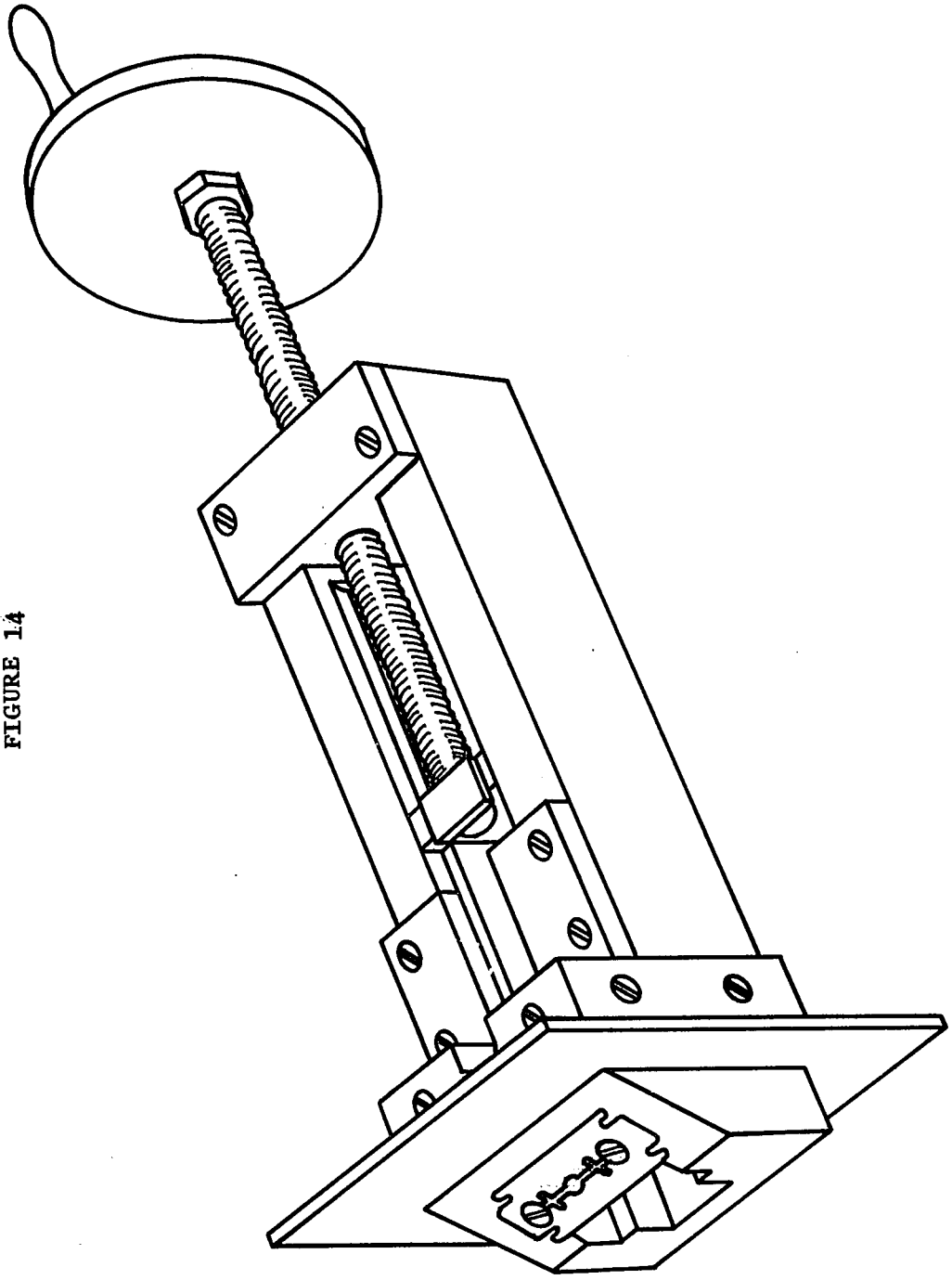

FIGURE 14

during casting. Since the atmosphere in the balance case could be maintained as desired, the nature of the casting atmosphere was held constant during the entire film forming process. Further, when the film is cast on the plate, the latter could be easily slid onto the pan of the balance, if desired. Consequently the time lag between casting and transfer of the plate to the pan of the balance was reduced to the minimum. To avoid end effects on film-dimensions during casting, films were cast continuously on three plates placed in series, and only the middle plate was used for evaporation rate measurements. The evaporation rate value is a function of the thickness of the cast solution layer, which under the same experimental conditions (use of the same casting plate) depends on the viscosity of the casting solution and on the casting speed. Therefore to get the comparable B data for different casting solutions several castings using differently grooved plates were made and the B values determined after 30 seconds of evaporation using the five-points formula. These improvements in technique resulted in more reproducible evaporation rate data. The measurements were made at the laboratory temperature (23-24^{o}C) with or without acetone vapor in the casting atmosphere. In the former case, the closed space of the balance case was kept in contact with the required concentration of aqueous acetone solution placed in a few shallow containers for at least an hour.

5. Determination of equilibrium phase separation data.

For the purpose of this determination, the casting solution was treated as a ternary system consisting of polymer (cellulose acetate), solvent (acetone), and nonsolvent (formamide). All compositions stated are in weight per cent. Solutions of different concentrations of cellulose acetate (20, 25, 30, 35%) were prepared. The polymer was first weighed in a 25 ml Erlenmeyer flask and formamide and acetone were then added by means of a syringe. Each flask was stirred at room temperature for 1 to 7 days to effect the maximum possible mixing of the components of the system. The turbidity caused by phase separation was recognized by visual observation which was easy for the system studied because of the clarity of the solutions involved. Formamide has been designated as "nonsolvent" just for the convenience of expressing compositions in the triangular diagram, and such designation does not imply that formamide has no solvent power for cellulose acetate.

FIGURE 15

COMPARATIVE PERFORMANCE OF BATCH 18 MEMBRANES

FIGURE 15

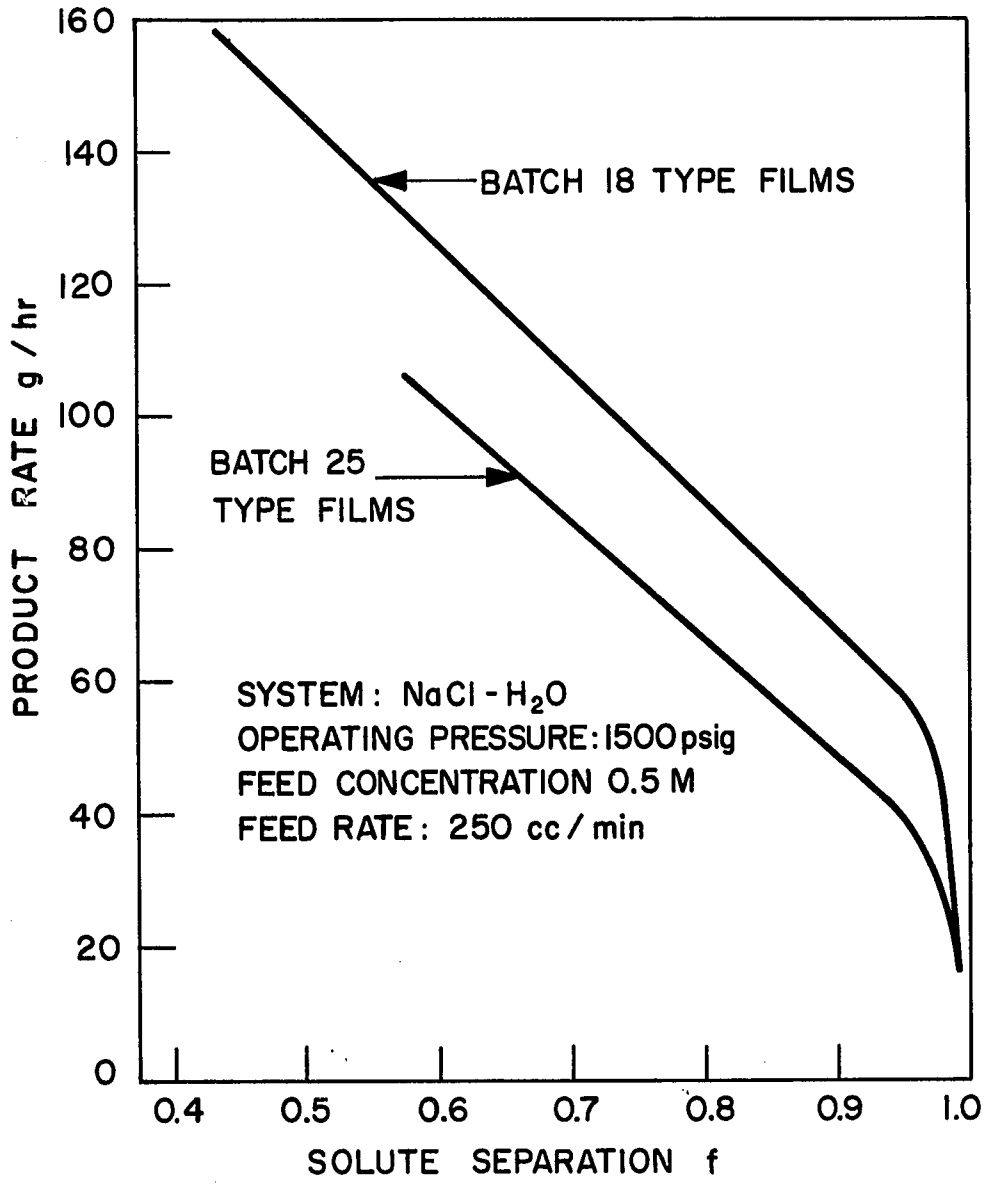
160
140
120
100
80
60
40
20
0
PRODUCT RATE g / hr
BATCH 18 TYPE FILMS
BATCH 25
TYPE FILMS
SYSTEM : NaCl - H2O
OPERATING PRESSURE: 1500 psig
FEED CONCENTRATION 0.5 M
FEED RATE : 250 cc / min
0.4
0.5
0.6
0.7
0.8
0.9
1.0
SOLUTE SEPARATION f

TABLE II

Film Casting Details for Formamide-Based Membranes (24)

Film casting details	Batch 47	Batch 400
Casting solution composition, wt.%		
Cellulose acetate (acetyl content 39.8%)	25	17
Acetone	45	56
Magnesium perchlorate	----	----
Water	----	----
Formamide	30	27
Casting solution temperature, ^{o}C	23-25	24
Temp. of casting atmosphere, ^{o}C	23-25	24
Casting atmosphere	ambient air	ambient air in contact with aqueous solution of 30 wt.% acetone
Solvent evaporation time, min.	1	0.5
Duration of film-setting in ice-cold water, hour	~1	>12
Nominal film thickness, inch	0.004	0.004

FIGURE 16

EFFECT OF COMPOSITION ON MEMBRANE CHARACTERISTIC CURVES AT AMBIENT AIR CASTING ATMOSPHERE

TABLE III

Casting Solution Composition of Some Formamide-Based Membranes

	B-47	B-403	B-400	B-401	B-402
Casting Solution Composition (wt.%)					
cellulose acetate (acetyl content 39.8%)	25	17	17	17	17
acetone	45	54	56	58	60
formamide	30	29	27	25	23

open cells which, together with the voids between cells, give rise to a microporous surface structure; on the other hand, in the interior bulk region of the film, the polymer molecules aggregate and precipitate rapidly giving rise to a spongy porous mass underneath the surface layer. The final result is the formation of a completely open celled asymmetric porous structure for the entire membrane.

3. Parameters affecting the nature of a membrane.

This model of the phase separation points out the importance of the state of the casting solution as well as the evaporation conditions during film formation which together affect the nature of the resulting membrane.

A) Structure of the casting solution. The term "the state of the casting solution" refers to the supermolecular polymer aggregation and formation of supermolecular structure that takes place in the concentrated cellulose acetate solutions (17). The structure of the casting solution is a function of composition and temperature, i.e. the size of polymer aggregates increases sharply with increase in polymer concentration and decrease in temperature (18). No effective means of expressing solution structures has yet been specified. However, useful conclusions seem possible from an analysis of the polymer-solvent-nonsolvent ternary phase equilibrium diagrams. For example, the remoteness of any point representing the composition of the casting solution from the phase boundary curve gives the

idea of the extent of supermolecular aggregation within the casting solution at particular temperature (25). Generally, less supermolecular aggregation and structurization within the casting solution makes possible the formation of more numerous smaller-size droplets of the dispersed phase in the surface region during solvent evaporation, which brings about the creation of more numerous micropores in the surface layer of resulting membrane.

B) Evaporation conditions. However, less supermolecular aggregation is not sufficient condition for obtaining more productive membranes. For the best performance the evaporation rate of the solvent should be appropriately adjusted to the state of casting solution. Solvent evaporation rate refers to the rate of solvent removal from the upper surface of the cast solution which ultimately forms the dense microporous layer in the resulting asymmetric membrane. This rate is a function of solution composition and temperature, of the ambient nature of the casting atmosphere and of its temperature. The solvent evaporation rate is decreased by a decrease in the temperature of the casting atmosphere and/or the presence of solvent vapor in the ambient casting atmosphere. For a given solution structure, an optimum solvent evaporation rate exists for best membrane performance.

4. Explanation of results.

Aa) Effect of the structure of the casting solution on the performance of the membranes. This general concept of the asymmetric reverse osmosis membrane formation mechanism gives us a basis for the explanation of the results shown in Fig. 2, and subsequent figures. For example, significantly higher productivities at the same level of separation for Batch 400 to Batch 403 membranes in comparison with that of Batch 47 membranes is obviously the result of the difference in the extent of supermolecular aggregation. This can be seen from the triangular diagram (Fig. 17) for the ternary system cellulose acetate-acetone-formamide. The compositions of the casting solutions B-47, B-400, B-401, B-402 and B-403 are represented by different points as in legend and the full line represents the phase boundary curve for the system cellulose acetate-acetone-formamide, i.e. the compositions at which the phase separation occurs. The compositions in the surface regions of the cast solutions change during solvent evaporation along the respective evaporation lines and the phase separation occurs when the composition in the surface region of particular solution reaches the point at the phase boundary curve. Since the distance of any particular point representing the casting solution composition from the phase boundary curve measures the extent of supermolecular aggregation within the solution, it can be concluded that the supermolecular aggregation in B-47 casting solution is significantly greater than those in B-400 series casting

FIGURE 17

LOCATION OF DIFFERENT BATCHES, THEIR EVAPORATION LINES AND THE PHASE BOUNDARY CURVE IN THE TERNARY EQUILIBRIUM DIAGRAM

FIGURE 17

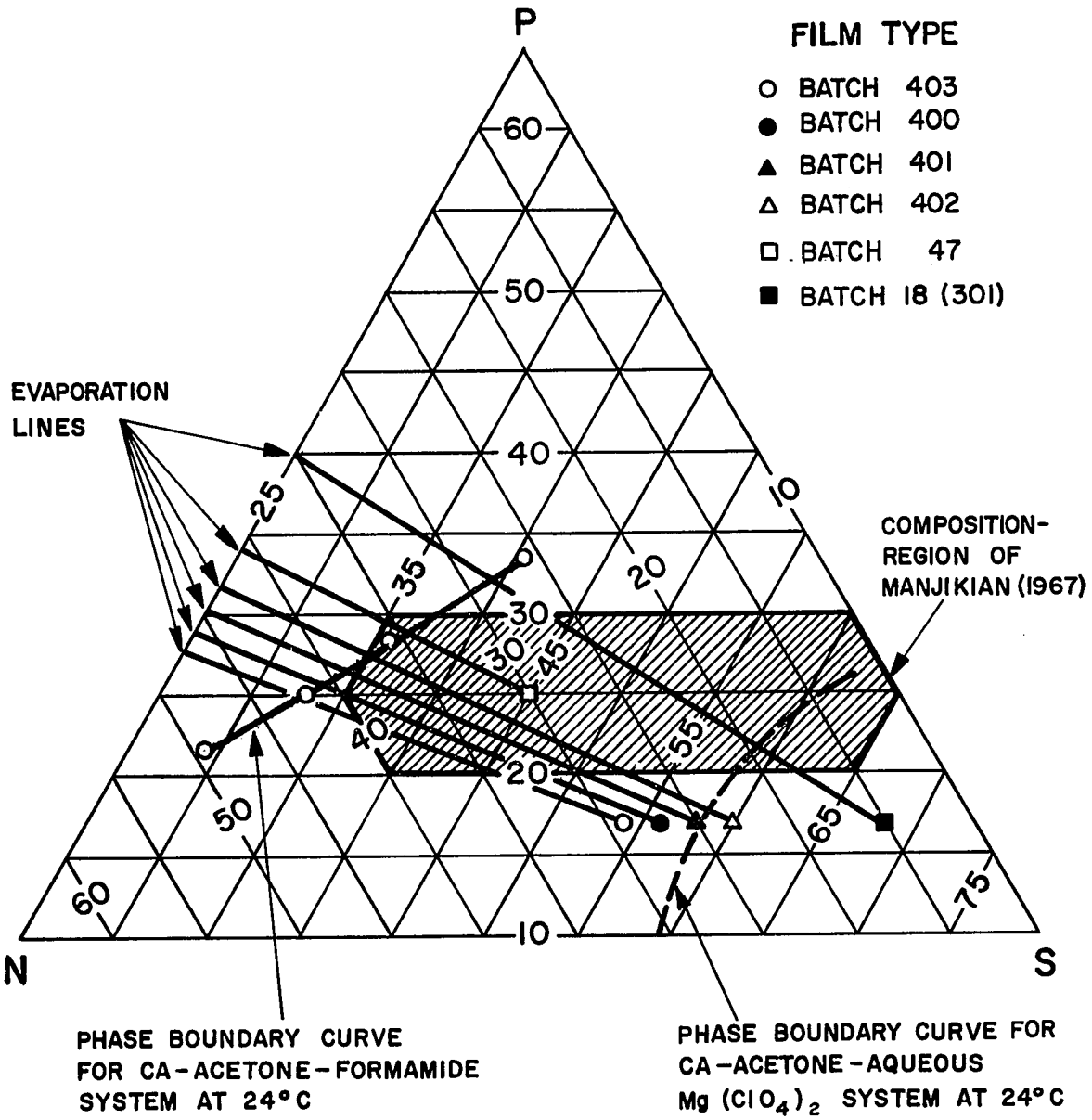
P
FILM TYPE
BATCH 403
BATCH 400
BATCH 401
BATCH 402
BATCH 47
BATCH 18 (301)
EVAPORATION LINES
COMPOSITION-REGION OF MANJIKIAN (1967)
60
50
40
30
20
10
25
35
45
55
65
75
N
S
PHASE BOUNDARY CURVE FOR CA-ACETONE-FORMAMIDE SYSTEM AT 24°C
PHASE BOUNDARY CURVE FOR CA-ACETONE-AQUEOUS Mg (ClO4)2 SYSTEM AT 24°C

solutions. Consequently, less numerous and bigger-size droplets of the dispersed phase should have been formed during solvent evaporation in the surface region of B-47 casting solution, which should result in the less numerous and bigger pores in the surface layer of formed membrane, i.e. in the less productive reverse osmosis membrane.

The mutual comparison of the performance (product rate vs solute separation) curves for the B-400, B-401, B-402 and B-403 membranes shows that the productivities of B-400 and B-401 membranes are superior to those of B-402 and B-403 ones. On the other hand, distances from the points representing the casting solutions to the phase boundary curve are in the order B-402>B-401>B-400>B-403, i.e. the order of their productivities differs from the order of the extent of supermolecular aggregation in the initial casting solutions. This only confirms the previously (23) expressed notion that the lower degree of supermolecular aggregation is not sufficient condition for obtaining more productive membranes, i.e. that this condition should be accompanied by the appropriate solvent evaporation rate.

Ab) Effect of the structure of the casting solution on the shrinkage temperature profile. The upper part of Fig. 16 and the other figures which will follow gives the membrane shrinkage temperature vs solute separation relationships (shrinkage temperature profile) and shows a relative measure of the pore size and pore size distribution on the membrane surface

in the as-cast condition. A higher shrinkage temperature to give a fixed level of solute separation would indicate a larger initial size of pores; a steeper shrinkage temperature profile would indicate less uniform pore size distribution. Applying these considerations to the shrinkage temperature profile curve in Fig. 16 one can see that the curve for the membranes cast from B-47 solution has a significantly different shape from those for the membranes of B-400 series. The B-47 membranes curve indicates the presence of a number of small pores nearly equal in size and a number of widely distributed big pores, noticeably bigger than the pores in the surface region of the B-402 type membranes. Such a pore size distribution is a direct consequence of the previously discussed influence of the extent of supermolecular aggregation in the casting solution. At the same time it affects the productivity of the B-47 membranes. As can be seen from the lower part of Fig. 16, lower membrane productivity results from the closure of small pores present in the as-cast condition of B-47 type membranes.

The comparison of the shrinkage temperature profile curves for membranes of B-400 series shows that the initial average pore size on the membrane surface (in the as-cast condition) decreases progressively in the order B-403 > B-400=B-401 > B-402, i.e. at the same cellulose acetate content in the casting solution it decreases with increasing the acetone fraction in solution. Considering this fact together with previously discussed

observation on the productivity variation with change in acetone content in the solution (productivity has a maximum value at intermediate acetone contents) one has to conclude that the membrane performance is affected by both the average pore size and the effective number of pores on the membrane surface.

B) Effect of Evaporation Conditions. Evaporation conditions during film formation expressed through the evaporation rate constitute the second important variable in the membrane formation process. Before discussing the effect of evaporation conditions on the membrane formation process it is necessary to show how evaporation rate measurements were evaluated.

a) Evaporation Rate Data. The general trend of the rapid decrease in solvent loss with time is expressed by the evaporation rate measurements which can be obtained by plotting the values of $(W_t - W_\infty)$ in grams vs t in seconds, where W_∞ represents the amount of casting solution remaining on the plate at infinite time and W_t, that remaining on the plate after t seconds. Assuming only acetone evaporates from the cast solution, one can plot $W_t - W_\infty$, the amount of acetone remaining on the plate t seconds after evaporation starts against time and calculate the evaporation rate as the negative value of the slope. A typical set of such data is plotted in the upper part of Fig. 18 which shows the decrease in acetone content in the casting solution with time. Its mirror image with respect to the time axis would represent the corresponding increasing amount

FIGURE 18

A) AMOUNT OF ACETONE REMAINING IN THE AS-CAST SOLUTION AFTER DIFFERENT TIMES OF EVAPORATION.

B) A TYPICAL EVAPORATION RATE CURVE.

(TEMPERATURE OF CASTING SOLUTION: 24^{o}C; CASTING ATMOSPHERE: AMBIENT AIR IN CONTACT WITH 80% WT. ACETONE SOLUTION; AREA OF EVAPORATION SURFACE: 8.15 cm^{2}).

of acetone evaporated with time from which the evaporation rate can be evaluated. Each curve of Fig. 18 indicates a decrease of evaporation rate with time. A more thorough analysis of the shape of the curve could lead to an understanding of the contribution of evaporation rate to the ultimate porous structure of the surface layer of the membrane.

The steep initial part of the curve probably indicates the constancy of the mechanism governing evaporation rate in the early stages of the process when it may be expected that the solvent loss from film surface is compensated by solvent diffusion to the film surface from underneath. In any case, since the cloud point (polymer phase separation) in the surface region may be expected to be reached soon after evaporation starts, the initial part of the curve is all important in representing the development of the formation of the porous structure of the surface region.

b) Factors affecting the evaporation rate value.

Preliminary results showed that, for a given casting solution composition and temperature, the relative position and slope of the initial part of the curve depended not only on evaporation conditions (temperature and acetone content of the casting atmosphere) but also on the thickness and surface area, S, of the film. As observed before, (25), a change in film thickness changes both the slope and relative position of the evaporation rate curve, whereas a change in surface area changes only the position but not the slope of the curve. The total quantity

FIGURE 19

EFFECT OF TEMPERATURE OF CASTING ATMOSPHERE ON EVAPORATION RATE

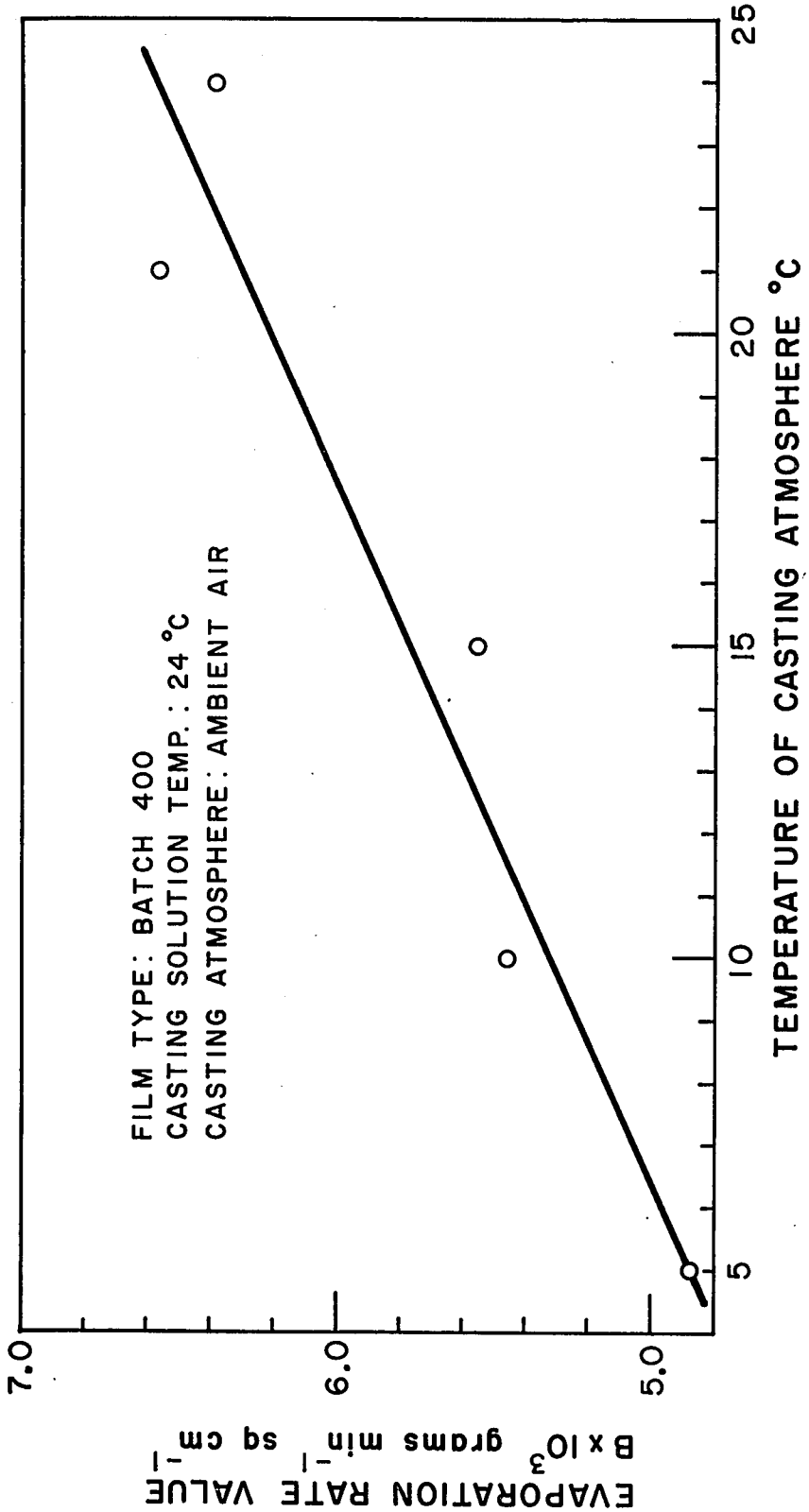
EVAPORATION RATE VALUE
B x 10³ grams min⁻¹ sq cm⁻¹
7.0
6.0
5.0
5
10
15
20
25
TEMPERATURE OF CASTING ATMOSPHERE °C
FILM TYPE: BATCH 400
CASTING SOLUTION TEMP.: 24 °C
CASTING ATMOSPHERE: AMBIENT AIR

FIGURE 19

Figure 20 gives the effect of the presence of acetone in the casting atmosphere on the value of B; these data correspond to the condition where the temperature of the casting solution and the temperature of the casting atmosphere were both at ambient laboratory condition ($24^{o}C$). These data show that the presence of acetone in the casting atmosphere reduces the value of B, and this reduction becomes progressively less steep with increasing saturation of the casting atmosphere with acetone. Thus the introduction of acetone in the casting atmosphere offers a sensitive means of reducing B which can be appropriately combined with the variation of the temperature of the casting atmosphere itself to suit particular needs.

c) Effect of evaporation rate on shrinkage temperature profile and performance of the membranes. The evaporation rate evaluated in this way and its variation affect both the membrane shrinkage temperature profiles and their performances. (Fig. 21 and 22, Table IV). The shrinkage temperature profiles of the B-403, B-400, B-401 and B-402 membranes get more widespread with the decrease of evaporation rates; the most noticeable is the change in shrinkage temperature profile of B-402 membranes, those of the B-400 and B-401 membranes are less marked and the shrinkage temperature profile of B-403 membranes practically does not change at all. This effect is a consequence of slowing down the pore formation process, the phenomenon which can be more easily recognized in the case of

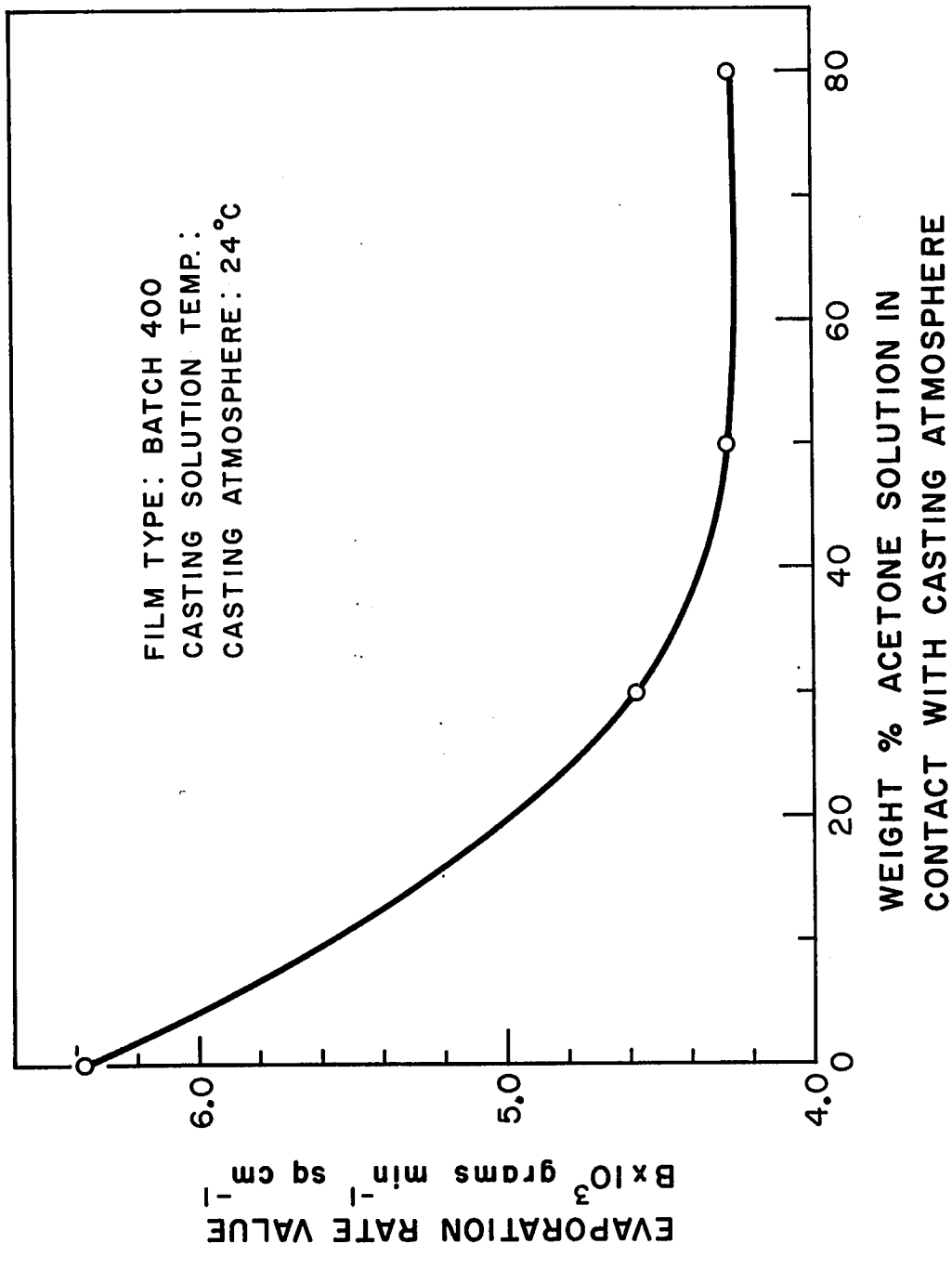
FILM TYPE: BATCH 400
CASTING SOLUTION TEMP.:
CASTING ATMOSPHERE: 24°C
EVAPORATION RATE VALUE
B x 10³ grams min⁻¹ sq cm⁻¹
6.0
5.0
4.0
0
20
40
60
80
WEIGHT % ACETONE SOLUTION IN
CONTACT WITH CASTING ATMOSPHERE

FIGURE 20

FIGURE 21

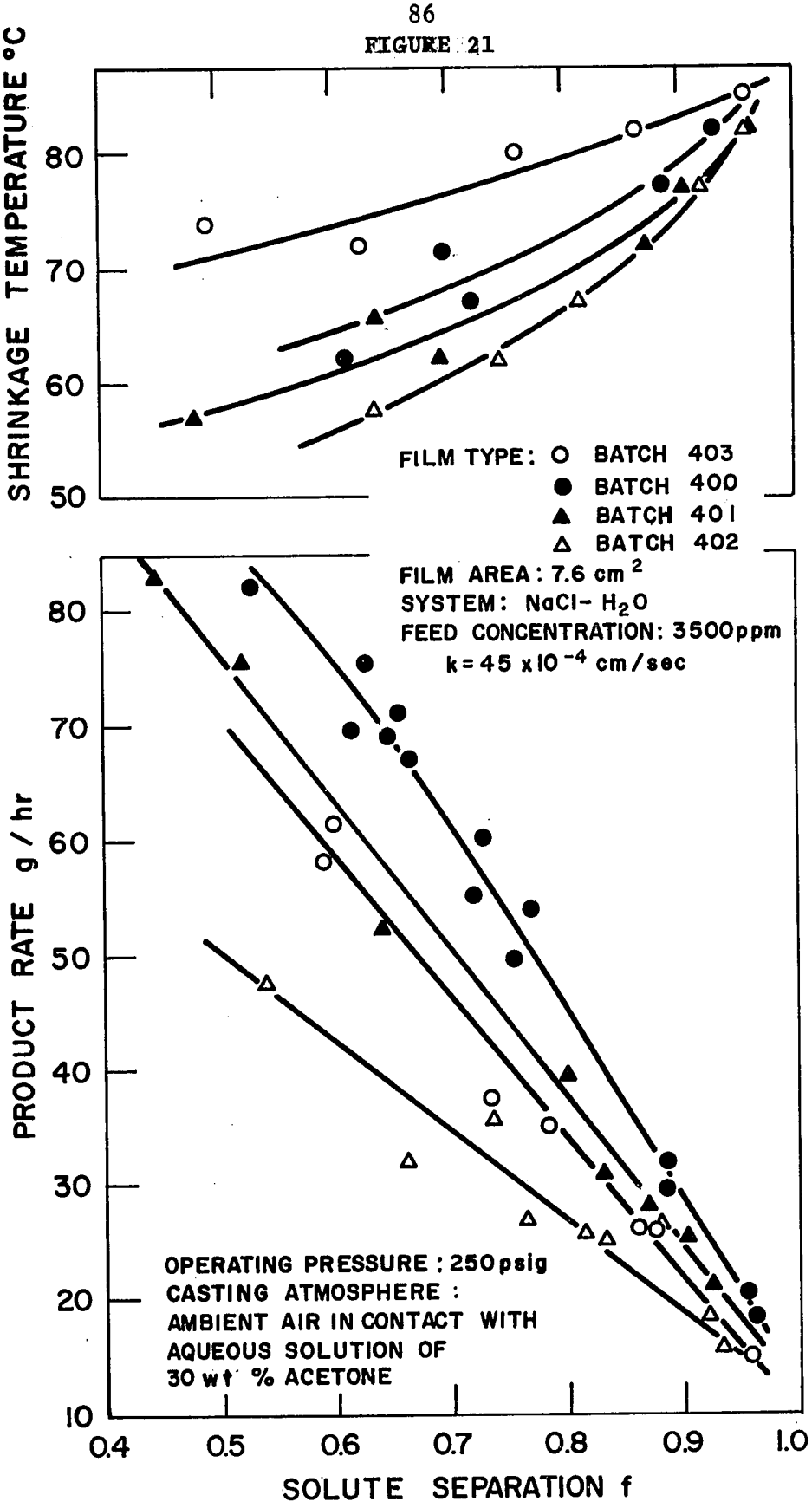
SHRINKAGE TEMPERATURE °C
80
70
60
50
FILM TYPE: ○ BATCH 403
● BATCH 400
▲ BATCH 401
△ BATCH 402
FILM AREA: 7.6 cm²
SYSTEM: NaCl- H₂O
FEED CONCENTRATION: 3500ppm
k = 45 x10⁻⁴ cm/sec
PRODUCT RATE g / hr
80
70
60
50
40
30
20
10
OPERATING PRESSURE: 250psig
CASTING ATMOSPHERE:
AMBIENT AIR IN CONTACT WITH
AQUEOUS SOLUTION OF
30 wt % ACETONE
0.4
0.5
0.6
0.7
0.8
0.9
1.0
SOLUTE SEPARATION f

FIGURE 22

EFFECT OF COMPOSITION ON THE CHARACTERISTIC CURVES OF MEMBRANES CAST UNDER AMBIENT AIR IN CONTACT WITH AN AQUEOUS SOLUTION OF 80 WT.% ACETONE

TABLE IV

Evaporation Rate Value, B (grams $min.^{-1}$, sq. $cm.^{-1}$)

at $\frac{W_{30} - W_{\infty}}{S}$ = 0.00429 grams/$cm.^2$

Weight % Acetone Solution in Contact with Casting Atmosphere	B-403	B-400	B-401	B-402
0	.00563	.00638	.00670	.00698
30	.00491	.00458	.00545	.00588
50	------	.00427	------	------
80	.00422	.00427	.00444	.00447

i.e. it resulted in more productive B-403, B-400 and B-401 membranes and slightly less productive B-402 ones. Further increase in the acetone vapor concentration in the casting atmosphere brought about, however, the drop in productivity showing that the evaporation rate was too slow. Thus from the point of view of productivity the B-400 type membranes cast in the air which was in contact with 30% aqueous acetone solution emerge as the best among all those studied.

Membrane performance is a function of both the average pore size and the effective number of pores on the membrane surface. Therefore the observed changes have to be related to variation of both factors. This means that knowing the direction of change in pore size, performance curves give an indication of the changes occuring in the effective number of pores as a result of changes in the evaporation rate. For instance, the decrease of evaporation rate value from .00638 to .00427 in the case of B-400 membranes has as a consequence the decrease of the initial average pore size on the membrane surface (Fig. 23). The simultaneous increase in membrane productivity makes possible only one conclusion to be derived and this is that effective number of pores on the surface has increased. Further decrease of evaporation rate does not change the average pore size in the cast membranes (see shrinkage profiles in Fig. 23), as the slight decrease of productivity indicates that the effective number of pores is

FIGURE 23

EFFECT OF THE PRESENCE OF ACETONE IN THE CASTING ATMOSPHERE ON THE CHARACTERISTIC CURVES OF BATCH 400 TYPE MEMBRANES

FIGURE 23

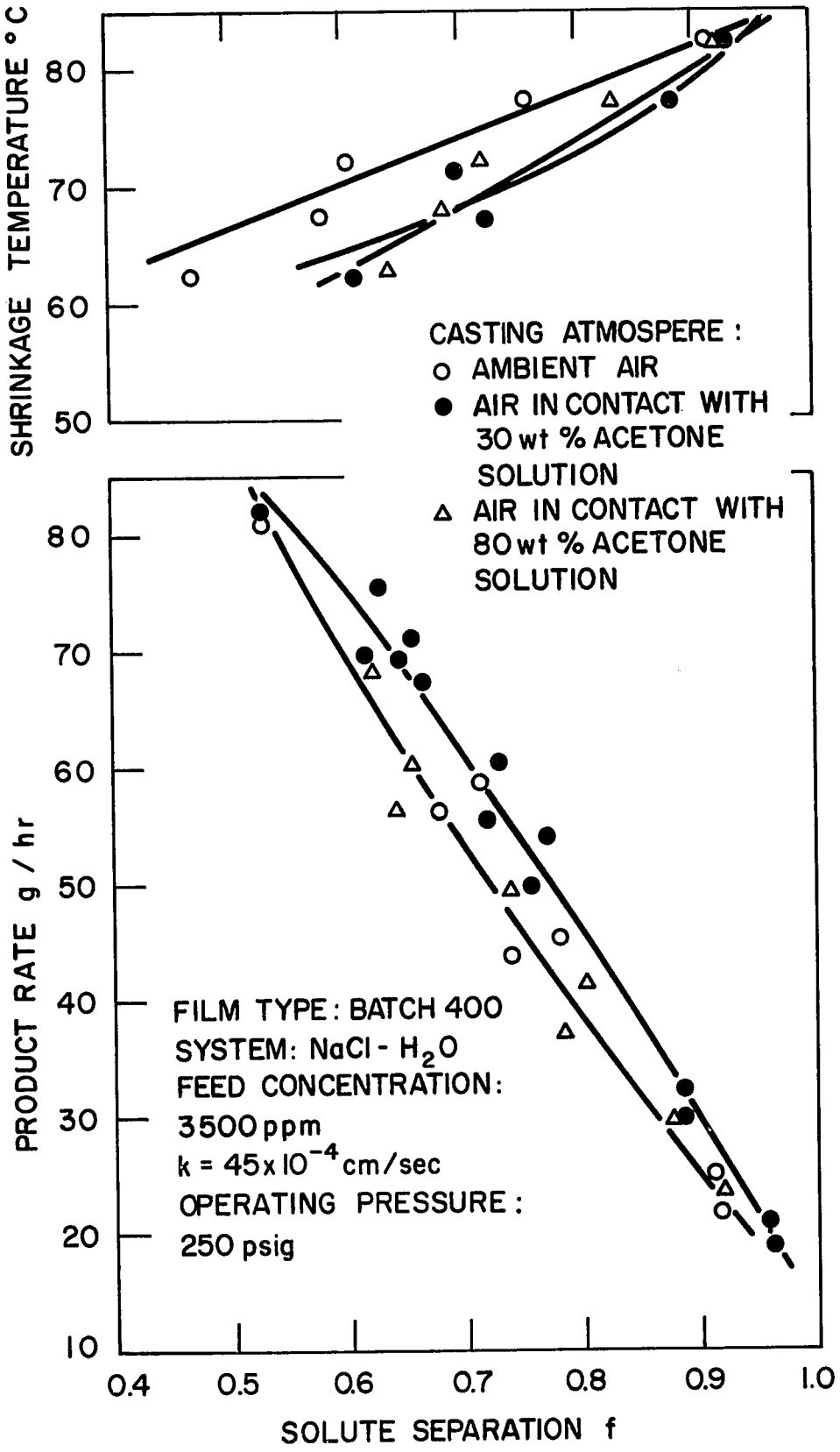
SHRINKAGE TEMPERATURE °C
80
70
60
50
CASTING ATMOSPERE :
○ AMBIENT AIR
● AIR IN CONTACT WITH 30 wt % ACETONE SOLUTION
△ AIR IN CONTACT WITH 80 wt % ACETONE SOLUTION
PRODUCT RATE g / hr
80
70
60
50
40
30
20
10
FILM TYPE : BATCH 400
SYSTEM: NaCl - H_2O
FEED CONCENTRATION:
3500 ppm
$k = 45 \times 10^{-4}$ cm/sec
OPERATING PRESSURE :
250 psig
0.4
0.5
0.6
0.7
0.8
0.9
1.0
SOLUTE SEPARATION f

insufficient to give the same productivity as in the case of membranes cast in the atmosphere in contact with 30% aqueous acetone solution. Similar considerations hold for the membranes cast from the other casting solutions.

d) Effect of evaporation period. Figure 24 illustrates the effect of evaporation period on shrinkage temperature profile and performance of Batch 400 type membranes. The longer the evaporation period, the bigger is the average size of initial pores on the membrane surface. This is understandable on the basis of the mechanism of pore formation discussed earlier (23), in which initially formed droplets in the surface region coalesce on prolongation of evaporation time forming larger ones which result eventually in bigger size pores on the membrane surface. Similar observations have been reported before with respect to Batch 18 type membranes (23). Unlike the latter type membranes however, evaporation period also affects the performance of Batch 400 type membranes. This is only to be expected in view of the less uniform smaller size pores obtained with Batch 400 membranes. It was found that an evaporation period of 30 seconds resulted in best membrane performance. Further, the data indicate that as the average size of pores on the membrane surface in the as-cast condition becomes smaller and smaller, one may expect an optimum evaporation period, and hence shrinkage temperature profile, for maximum membrane productivity.

FIGURE 24

EFFECT OF EVAPORATION PERIODS ON THE

CHARACTERISTIC CURVES OF BATCH 400 TYPE MEMBRANES

FIGURE 24

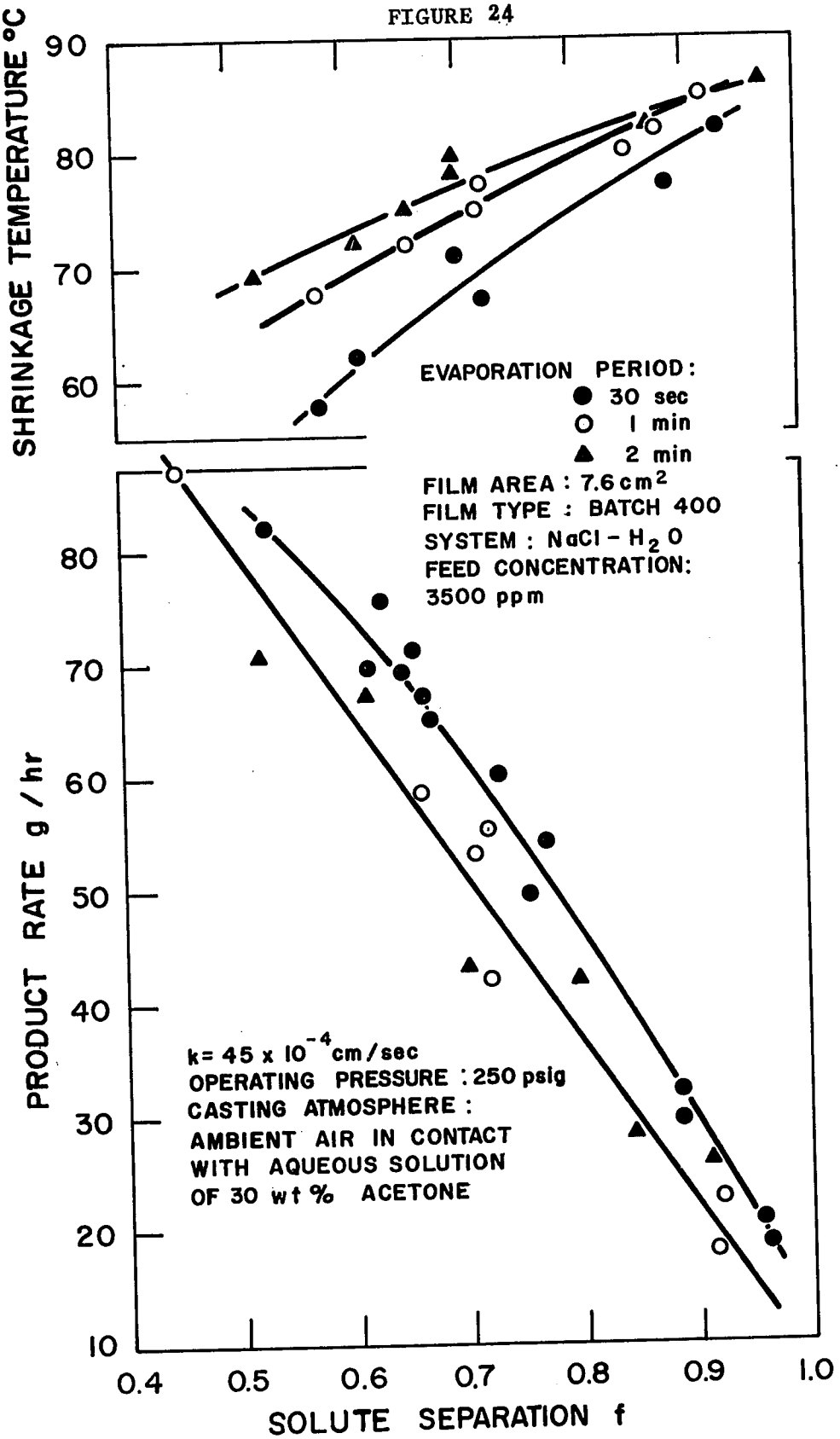
SHRINKAGE TEMPERATURE °C
90
80
70
60
EVAPORATION PERIOD:
30 sec
1 min
2 min
FILM AREA : 7.6 cm²
FILM TYPE : BATCH 400
SYSTEM : NaCl - H₂O
FEED CONCENTRATION:
3500 ppm
PRODUCT RATE g / hr
80
70
60
50
40
30
20
10
k= 45 x 10⁻⁴ cm/sec
OPERATING PRESSURE : 250 psig
CASTING ATMOSPHERE :
AMBIENT AIR IN CONTACT
WITH AQUEOUS SOLUTION
OF 30 wt % ACETONE
0.4
0.5
0.6
0.7
0.8
0.9
1.0
SOLUTE SEPARATION f

e) Significance of evaporation rate. The significance of evaporation rate as a controlling parameter in the development of the porous structure of the membrane surface may be brought out by yet another consideration. The casting condition of B-400 type membranes given in Table II is taken here for illustration. Referring to Fig. 20, the value of B equals (0.00458) corresponding to casting atmosphere at 24°C in contact with an aqueous solution of 30% acetone; referring to Fig. 19, the same value of B is obtained at 2.0°C ambient air casting atmosphere without any acetone. These two casting conditions are hence equivalent. Consequently, using a casting solution temperature of 24°C, membranes cast in acetone free ambient air at 2.0°C may be expected to yield the same performance curves (solute separation-product rate correlation) as that given by the Batch 400 membranes at casting conditions as in Table II. After many trials, this could not be shown since the shrinkage temperature profile could not be reached.(Fig.25)

It has been shown that the shrinkage temperature profile is a function of evaporation time, and it does not affect the solute separation-product rate correlation (performance curve) for Batch 18 type films which contain comparatively big and uniform surface pores. Batch 400 films however contain smaller and less uniform pores; for these films, it is only reasonable to expect that a shift in the shrinkage temperature profile (which expresses pore size distribution) will also shift the membrane performance curve. Consequently, reproductibility of

FIGURE 25

COMPARATIVE PERFORMANCE AND SHRINKAGE PROFILE OF BATCH 400 MEMBRANES CAST AT DIFFERENT AMBIENT AIR TEMPERATURES

the performance of Batch 400 membranes should also depend on reproducing their shrinkage temperature profile. As observed earlier, films whose shrinkage temperature profile data are not too far separated, exhibit essentially identical membrane performance. This observation is one of fundamental significance from the point of view of quality control in making reverse osmosis membranes.

5. Comparison of results.

The results presented so far and the discussion following them showed the practical importance of the general approach based on the solution structure-evaporation rate concept for creating more productive formamide-based reverse osmosis membranes. This can be clearly illustrated by the comparison of B-400 membranes which represent the best heretofore produced formamide-based membranes with magnesium perchlorate-based B-316 membranes introduced earlier (24)(Fig. 11 and 26). Both figures show that formamide-based membranes of adequate performances to those produced from magnesium perchlorate-cellulose acetate-acetone-water solutions for low, medium and high pressures can be obtained, although shrinkage temperature profile curves show slightly larger pore size in the B-400 membranes what might indicate certain differences in the number of pores obtained in the surface area of the as-cast membranes. Anyway, the productivities of B-400 membranes at 90% level of solute separation and feed flow conditions corresponding to a mass transfer co-

FIGURE 26

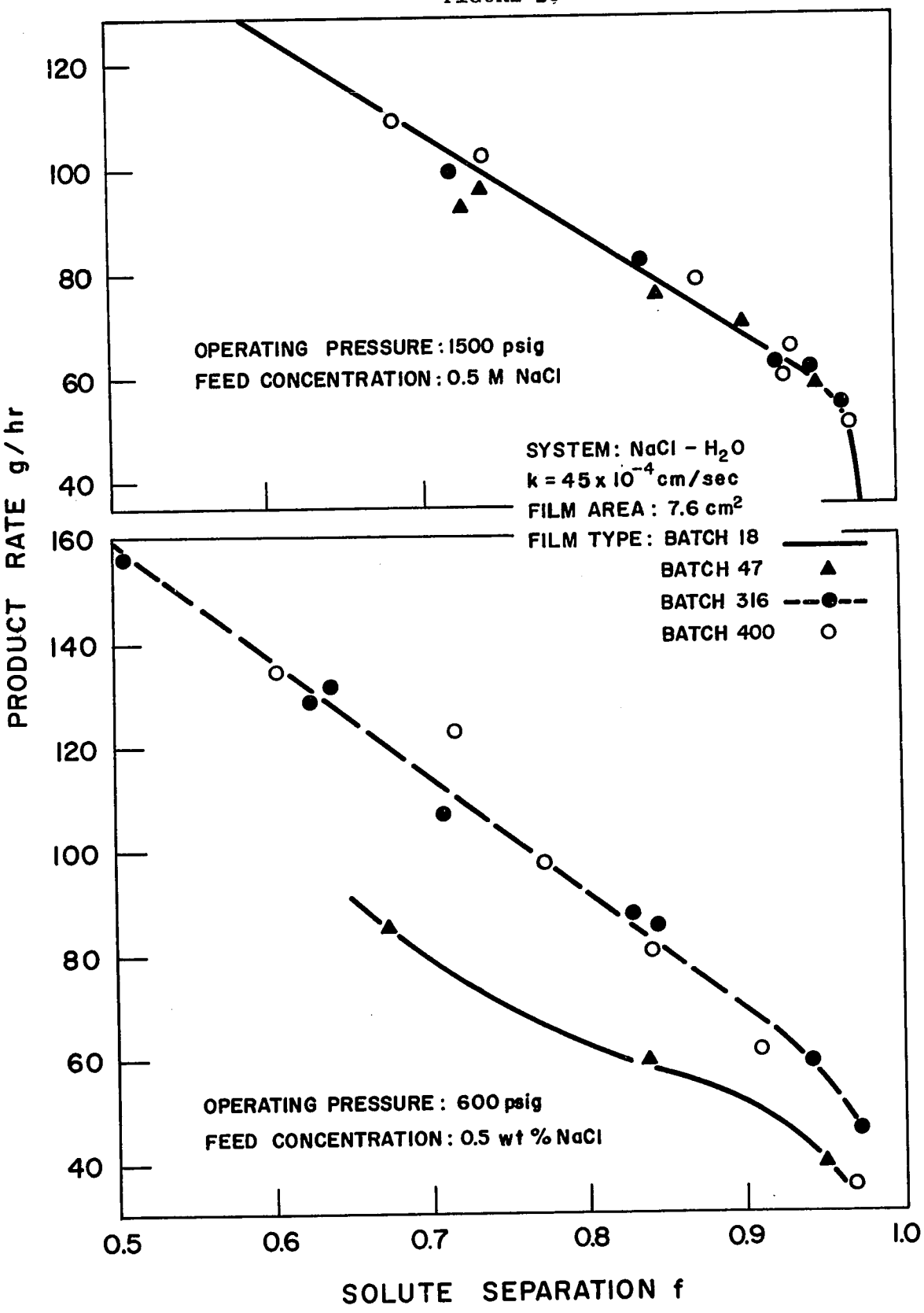
PRODUCT RATE g/hr
SOLUTE SEPARATION f
OPERATING PRESSURE: 1500 psig
FEED CONCENTRATION: 0.5 M NaCl
SYSTEM: NaCl - H2O
k = 45 x 10^-4 cm/sec
FILM AREA: 7.6 cm2
FILM TYPE: BATCH 18
BATCH 47
BATCH 316
BATCH 400
OPERATING PRESSURE: 600 psig
FEED CONCENTRATION: 0.5 wt % NaCl
120
100
80
60
40
160
140
120
100
80
60
40
0.5
0.6
0.7
0.8
0.9
1.0

TABLE V

Membrane Performances During Continuous Reverse Osmosis Operation (24)

System : $NaCl-H_2O$

Operating Pressure: 600 psig

Feed Concentration: 0.5 wt.% NaCl

k : 45×10^{-4} cm/sec.

Film Area : 7.6 cm^2

Start		After 24 hours			After 72 hours		
$[PR]_1$ g./hr.	$fx10^2$	$[PR]_2$ g./hr.	$fx10^2$	$\frac{[PR]_2}{[PR]_1} x10^2$	$[PR]_3$ g./hr.	$fx10^2$	$\frac{[PR]_3}{[PR]_1} x10^2$
59.94	91.2	52.16	91.2	87.0	52.44	89.5	87.5
79.54	84.1	68.69	85.5	86.4	68.34	83.7	85.9
121.48	69.3	104.12	73.5	85.7	101.34	66.9	83.4
134.64	59.3	113.12	63.8	84.0	110.14	58.5	81.8
Film Type CA-NRC-400							
68.19	87.0	62.38	87.4	91.5	62.54	86.3	91.7
68.10	86.3	62.21	86.7	91.4	62.26	85.2	91.4
101.32	68.5	90.38	69.7	89.2	89.04	67.3	87.9
110.13	68.7	97.47	70.8	88.5	95.17	66.7	86.4
Film Type CA-NRC-316							

CONCLUSIONS

The results obtained with the class of membranes investigated in this project lead to significant conclusions in the development of more productive reverse osmosis membranes. The state or the structure of the casting solution and the rate of solvent evaporation during film formation were found to constitute an important interconnected variable governing the ultimate porous structure, and hence the performance of the resulting membranes in reverse osmosis.

The performance of the formamide-based membranes increases with decrease of cellulose acetate content in the casting solution. From the point of view of productivity the B-400 type membranes cast in the air which was in contact with 30% aqueous acetone solution emerge as the best among all those studied. This only confirms the earlier observed notion (23) that to a certain casting solution structure should correspond the appropriate evaporation rate. The latter were found to decrease by decreasing the casting atmosphere temperature or in the presence of acetone in the casting atmosphere. The effect of evaporation period was also studied and a short evaporation time proved to give more productive membranes.

LITERATURE CITED (CONT'D)

11. Kimura, S., and Sourirajan, S., AIChE J., 13, 497 (1967).

12. Kimura, S., and Sourirajan, S., Ind. Eng. Chem. Process Design Develop., 7, 41 (1968).

13. Kimura, S., and Sourirajan, S., ibid., 7, 197 (1968).

14. Kimura, S., and Sourirajan, S., ibid., 7, 539 (1968).

15. Kimura, S., and Sourirajan, S., ibid., 7, 548 (1968).

16. Kimura, S., Sourirajan, S., and Ohya, H., Ind. Eng. Chem. Process Design Develop., 8, 79 (1969).

17. Klenin, V. I., and Kolnibolotchuk, N. K., Mekh. Protsessov Plenkoobrazov. Polim. Rastvorov Dispersii, Akad. Nauk SSSR, Sb. Statei, 32 (1966).

18. Klenin, V. I., and Klenina, O. V., Mekh. Protsessov Plenkoobrazov. Polim. Rastvorov Dispersii, Akad. Nauk SSSR, Sb. Statei, 45 (1966).

19. Kopeček, J., and Sourirajan, S., J. Appl. Polym. Sci., 13, 637 (1969).

20. Kopeček, J., and Sourirajan, S., "Performance of Porous Cellulose Acetate Membranes for the Reverse Osmosis Separation of Mixtures of Organic Liquids," Paper submitted to Ind. Eng. Chem. Process Design Develop. (1969).

21. Kopeček, J., and Sourirajan, S., Can. J. Chem. 47, 3467 (1969).

22. Kopeček, J., and Sourirajan, S., Ind. Eng. Chem. Prod. Res. Develop. 8, 274 (1969).

23. Kunst, B., and Sourirajan, S., J. Appl. Polymer Sci., 14, 723 (1970).

LITERATURE CITED (CONT'D)

24. Kunst, B., and Sourirajan, S., "Development and Performance of Some Porous Cellulose Acetate Membranes for Reverse Osmosis Desalination", J. Appl. Polym. Sci. (in press).

25. Kunst, B., and Sourirajan, S., "Evaporation Rate and Equilibrium Phase Separation Data in Relation to Casting Conditions and Performance of Porous Cellulose Acetate Reverse Osmosis Membranes," J. Appl. Polym. Sci. (in press).

26. Loeb, S., and Sourirajan, S., in "Sea Water Research," Department of Engineering, University of California, Los Angeles, Report No. 59-3 (1958).

27. Loeb, S., and Sourirajan, S., in "Sea Water Research," Department of Engineering, University of California, Los Angeles, Report No. 59-28 (1959).

28. Loeb, S., and Sourirajan, S., ibid., Report No. 59-46 (1959).

29. Loeb, S., and Sourirajan, S., ibid., Report No. 60-5 (1960).

30. Loeb, S., and Sourirajan, S., ibid., Report No. 60-26 (1960).

31. Loeb, S., and Sourirajan, S., "Sea Water Demineralization By Means of a Semipermeable Membrane," Department of Engineering, University of California, Los Angeles, Report No. 60-60 (1961).

32. Loeb, S., and Sourirajan, S., Advan. Chem. Ser., No. 38, 117 (1963).

LITERATURE CITED (CONT'D)

33. Loeb, S., and Sourirajan, S., U.S. Patent 3,133,132 (May 12, 1964).

34. Loeb, S., and Sourirajan, S., U.S. Patent 3,223,424 (Dec. 14, 1965).

35. Loeb, S., Sourirajan, S., and Weaver, D. E., U.S. Patent 3,133,137 (May 12, 1964).

36. Lonsdale, H. K., in "Desalination by Reverse Osmosis," U. Merten, Ed., Chap. 4, The M.I.T. Press, Cambridge, Mass., 1966.

37. Lonsdale, H. K., Merten, U., and Riley, R. L., J. Appl. Polym. Sci., 9, 1341 (1965).

38. Lonsdale, H. K., Merten, U., Riley, R. L., Vos, K. D., and Westmoreland, J. C., "Reverse Osmosis for Water Desalination," U.S. Dept. Interior, Office of Saline Water, Research and Development Progress Report No. 111 (1964).

39. Lonsdale, H. K., Merten, U., and Tagami, M., J. Appl. Polym. Sci., 11, 1807 (1967).

40. Manjikian, S., Loeb, S., and McCutchan, J. W., Proc. First International Symp. on Water Desalination, Washington, D.C., 1965. (Pub. U.S. Dept. Interior, Office of Saline Water, Washington, D.C., Vol. 2, p 159-73).

41. Meares, P., Eur. Polym. J., 2, 241 (1966).

42. Michaels, A. S., Bixler, H. J., and Hodges, R. M., Jr., J. Colloid Sci., 20, 1034 (1965).

43. Reid, C. E., and Breton, E. J., J. Appl. Polym. Sci., 1, 133 (1959).

APPENDIX

TABLE VI

Conditions of Casting: 30 Sec., 30% Acetone Vapor

Shrinkage Temp.	403 (29F)			Shrinkage Temp.	400 (27F)		
(°C)	PWP (g/hr.) (25°C)	PR (g/hr.) (25°C)	% Salt Removed	(°C)	PWP (g/hr.) (25°C)	PR (g/hr.) (25°C)	% Salt Removed
88	10.22	8.20	97.83	82	26.12	20.67	95.53
85	18.5	15.1	95.75	82	21.58	17.7	94.21
82	32.14	25.84	87.39	82	22.99	18.38	95.88
82	40.83	32.52	85.47	82	37.44	29.43	87.35
82	33.05	26.2	86.25	77	40.1	31.8	88.5
80	42.55	34.85	78.40	77	33.1	26.25	88.92
80	44.70	37.33	73.53	77	36.6	29.5	88.5
77	44.7	45.0	66.25	72	66.15	55.2	71.88
77	71.6	58.02	59.01	72	60.45	46.00	77.1
74	83.45	69.8	49.3	72	85.8	69.3	61.50
72	75.8	61.6	65.1	67	64.8	53.95	76.55
72	93.9	75.0	62.5	67	76.45	60.25	72.75
72	74.08	61.71	59.96	67	60.7	49.4	75.35
67	114.4	95.9	43.1	67	82.0	66.9	65.82
				62	78.6	67.1	66.42
				62	86.3	69.25	64.7
				62	98.6	81.8	52.75
				58	112.98	95.24	45.56
				57	88.41	75.51	62.73
				57	85.07	70.79	65.48

TABLE VII

Conditions of Casting: 30 Sec., 80% Acetone Vapor

Shrinkage Temp.	$403_{(29F)}$				$400_{(27F)}$		
(°C)	PWP (g/hr.) (25°C)	PR (g/hr.) (25°C)	% Salt Removed	(°C)	PWP (g/hr.) (25°C)	PR (g/hr.) (25°C)	% Salt Removed
90	9.95	8.40	97.61	82	28.64	23.26	91.85
85	24.3	20.1	90.75	77	45.8	36.1	78.25
82	35.28	29.26	78.93	77	38.3	29.65	87.55
82	35.43	29.18	78.87	72	52.7	41.0	79.95
78	42.8	35.8	77.35	72	68.55	56.0	64.04
77	41.5	34.8	76.0	67	61.7	49.05	73.55
75	61.7	50.8	71.8	66	76.9	65.0	63.90
75	66.0	55.0	62.18	62.6	74.1	60.25	65.3
72	81.9	69.5	57.85	62	83.9	68.85	62.27
72	85.4	71.9	56.2				
	$401_{(25F)}$				$402_{(23F)}$		
82	18.12	14.85	96.22	82	10.39	8.43	97.38
82	28.70	23.68	88.35	82	14.63	11.92	96.31
77	22.8	18.8	91.92	77	20.3	16.9	87.60
77	29.0	23.85	92.35	77	18.62	15.38	92.66
72	39.0	31.65	87.74	72	23.0	18.45	91.02
72	39.25	32.0	85.35	72	22.95	18.53	91.57
68	46.0	38.0	81.22	67	23.35	18.92	90.62
67	54.3	44.7	79.66	66	23.0	18.70	89.31
62.8	64.3	51.25	67.8	63	29.88	24.40	85.15
62	62.3	53.7	60.40	62	26.75	22.08	84.28
57.5	82.88	72.92	48.25	57	52.65	44.51	66.63
57	66.75	56.13	64.58	57	43.72	36.63	73.53

TABLE VIII

Conditions of Casting: 30 Sec., No Acetone Vapor

Shrinkage Temp.	$403_{(29F)}$				$400_{(27F)}$		
(°C)	PWP (g/hr.) (25°C)	PR (g/hr.) (25°C)	% Salt Removed	(°C)	PWP (g/hr.) (25°C)	PR (g/hr.) (25°C)	% Salt Removed
88	10.96	8.95	97.73	82	26.6	20.9	91.67
85	19.3	15.8	96.45	82	30.08	24.20	91.47
82	41.02	33.45	82.23	77	53.2	42.8	73.95
82	51.36	41.32	67.39	77	55.4	44.85	78.1
82	36.03	30.49	82.02	72	69.2	56.0	68.0
82	45.3	36.8	73.8	72	97.0	80.80	53.13
79	54.65	44.75	68.9	67	88.3	72.7	58.4
77	39.65	32.6	84.75	62	73.7	58.55	71.48
77	108.42	87.2	35.7	62	169.0	150.2	22.92
74	91.1	76.9	50.88				
72	91.97	77.80	49.83				
	$401_{(25F)}$				$402_{(23F)}$		
82	16.45	13.34	96.01	82	14.34	11.74	96.88
82	32.97	26.49	89.06	82	18.13	14.84	96.14
82	32.77	26.24	90.15	77	15.73	13.12	95.79
77	26.0	21.25	92.63	77	35.25	29.18	82.80
77	54.2	44.25	73.80	72	31.88	26.12	87.95
72	89.45	76.3	57.8	67	53.85	44.80	72.52
72	93.4	79.6	49.7	66	44.0	37.5	71.1
67	148.7	134.4	32.6	62	33.9	28.82	79.9
67	143.4	127.2	28.48	62	55.10	47.0	63.96
66	52.1	42.55	80.93	57	105.21	94.11	33.77
62	96.4	82.65	53.90				
62	155.2	143.1	27.33				
62	113.0	98.9	40.03				
57	104.08	92.14	43.26				
57	174.90	162.65	21.17				
57	160.47	141.68	28.47				

TABLE IX

Conditions of Casting: 30 Sec., No Acetone Vapor

B-400

Shrinkage Temp.	Air at 5°C			Shrinkage Temp.	Air at 18°C		
(°C)	PWP (g/hr.) (25°C)	PR (g/hr.) (25°C)	% Salt Removed	(°C)	PWP (g/hr.) (25°C)	PR (g/hr.) (25°C)	% Salt Removed
82	31.95	25.60	89.14	82	31.72	25.42	90.51
82	30.73	24.25	93.48	74	76.13	59.56	67.84
72	91.02	76.65	52.21				
72	92.73	74.40	58.15				
72	98.85	80.74	50.38				

TABLE X

Effect of Evaporation Period on Shrinkage Temperature Profile

Shrinkage Temp.	% Salt Removed		
(°C)	B-400 - (1) (30 sec.)	B-400 - (2) (1 min.)	B-400 - (3) (2 min.)
90		97.82	98.0
86			97.1
85		91.40	
82	93.24	87.60	87.35
80		84.98	70.1
78			70.1
77	88.64	72.40	
75		72.05	65.90
72	70.16	66.05	61.3
69			52.5
67.5		57.75	
67	72.62		
65			24.5
62.3		41.75	
62	61.29		
60		38.35	
57.3	57.92		
57		41.85	

TABLE XII

EVAPORATION RATE MEASUREMENTS

Casting solution: B-403

Conditions of atmosphere: 24°C; 30 wt.% acetone vapor

Plate Number	10	13	13	16
Weight of empty plate (grams)	58.6911	57.7027	57.7071	57.7054
Evaporation period (seconds)	Weight of plate + casting solution (grams)			
20	58.7820	57.8308	57.8161	57.8582
30	58.7760	57.8238	57.8094	57.8507
45	58.7697	57.8150	57.8017	57.8414
60	58.7659	57.8083	57.7957	57.8340
75	58.7637	57.8031	57.7926	57.8282
90	58.7625	57.7993	57.7898	57.8237
105	58.7618	57.7967	57.7878	57.8198
120	58.7615	57.7948	-------	57.8169
150	58.7613	57.7924	57.7853	57.8129
180	58.7613	57.7913	57.7846	57.8105
240		57.7906	57.7845	57.8083
300		57.7906	57.7845	57.8078
360				57.8078
$W_{30} - W_{\infty}$(grams)	0.0147	0.0332	0.0249	0.0429
B (grams $min.^{-1}$, sq. cm^{-1})	0.00382	0.00481	0.00442	0.00521

Casting solution: B-400

Conditions of atmosphere: 24°C; 0 wt.% acetone vapor

Plate Number	10	13	16
Weight of empty plate (grams)	58.6908	57.6869	57.6860
Evaporation period (seconds)	Weight of plate + casting solution (grams)		
20	58.7530	57.7987	57.8319
30	58.7464	-------	57.8222
45	58.7410	57.7782	57.8108
60	58.7385	57.7711	57.8017
75	58.7373	57.7661	57.7941
90	58.7368	57.7630	57.7892
105	58.7365	57.7610	57.7852
120	58.7365	57.7596	57.7822
150		57.7582	57.7781
180		57.7575	57.7758
240		57.7573	57.7737
300		57.7573	57.7731
360			57.7731
$W_{30} - W_{\infty}$(grams)	0.0099	0.0318	0.0491
B (grams $min.^{-1}$, sq. cm^{-1})	0.00380	0.00631	0.00653

Casting solution: B-400

Conditions of atmosphere: 24°C; 30 wt.% acetone vapor

Plate Number	10	13	16
Weight of empty plate (grams)	58.6882	57.6963	57.7008
Evaporation period (seconds)	Weight of plate + casting solution (grams)		
20	58.7722	57.8311	57.8453
30	58.7670	57.8242	57.8380
45	58.7608	57.8156	57.8285
60	58.7569	57.8087	57.8212
75	58.7546	-------	57.8155
90	58.7532	57.7991	57.8109
105	58.7524	57.7954	57.8073
120	58.7521	57.7932	57.8047
150	58.7519	57.7901	57.8009
180	58.7519	57.7883	57.7985
240		57.7869	57.7965
300		57.7868	57.7960
360		57.7868	57.7960
$W_{30} - W_{\infty}$ (grams)	0.0151	0.0374	0.0420
B (grams $min.^{-1}$, sq. cm^{-1})	0.00355	0.00477	0.00518

Casting solution: B-400

Conditions of atmosphere: 24°C; 80 wt.% acetone vapor

Plate Number	10	13	16
Weight of empty plate (grams)	58.7012	57.7207	57.7242
Evaporation period (seconds)	Weight of plate + casting solution (grams)		
20	58.7938	57.8418	57.8709
30	58.7886	57.8359	57.8647
45	58.7832	57.8282	57.8563
60	58.7798	57.8226	57.8497
75	58.7779	57.8181	57.8443
90	58.7768	57.8148	57.8398
105	58.7762	57.8122	57.8364
120	58.7758	57.8104	57.8336
150	58.7757	57.8082	57.8296
180	58.7757	57.8070	57.8271
240		57.8063	57.8246
300		57.8063	57.8239
360			57.8238
420			57.8238
$W_{30} - W_{\infty}$ (grams)	0.0129	0.0296	0.0409
B (grams $min.^{-1}$, sq. cm^{-1})	0.00334	0.00412	0.00443

Casting solution: B-401

Conditions of atmosphere: 24°C; 0 wt.% acetone vapor

Plate Number	10	13	16
Weight of empty plate (grams)	58.6959	57.6925	57.6912
Evaporation period (seconds)	Weight of plate + casting solution (grams)		
20	58.7609	57.8038	-------
30	58.7528	57.7939	57.8128
45	58.7453	57.7824	57.8006
60	58.7417	57.7743	57.7917
75	58.7402	57.7688	57.7854
90	58.7395	57.7652	57.7807
105	58.7393	57.7629	57.7776
120	58.7392	57.7615	57.7753
150	58.7392	57.7600	57.7725
180		57.7593	57.7710
240		57.7590	57.7698
300		57.7590	57.7696
360			57.7696
$W_{30} - W_{\infty}$(grams)	0.0136	0.0349	0.0432
B (grams $min.^{-1}$, sq. cm^{-1})	0.00496	0.00670	0.00659

Casting solution: B-401

Conditions of atmosphere: 24°C; 30 wt.% acetone vapor

Plate Number	10	13	16
Weight of empty plate (grams)	58.6946	57.7013	57.7054
Evaporation period (seconds)	Weight of plate + casting solution (grams)		
15	-------	-------	57.8588
20	58.7692	57.8222	-------
30	58.7636	57.8148	57.8462
45	58.7570	57.8043	57.8354
60	58.7534	57.7970	57.8272
75	58.7517	57.7916	57.8206
90	58.7507	57.7877	57.8151
105	58.7502	57.7848	57.8108
120	58.7500	57.7828	57.8075
150	58.7500	57.7807	57.8028
180		57.7796	57.8001
240		57.7792	57.7976
300		57.7792	57.7970
360			57.7970
$W_{30} - W_{\infty}$(grams)	0.0136	0.0356	0.0492
B (grams $min.^{-1}$, sq. cm^{-1})	0.00378	0.00548	0.00580

Casting solution: B-402

Conditions of atmosphere: 24°C; 0 wt.% acetone vapor

Plate Number	10	13	16
Weight of empty plate (grams)	58.6946	57.6924	57.6924
Evaporation period (seconds)	Weight of plate + casting solution (grams)		
15	58.7582	-------	-------
20	-------	57.7982	-------
30	58.7456	-------	57.8108
45	58.7396	57.7762	57.7986
60	58.7372	57.7682	57.7890
75	58.7363	57.7632	57.7824
90	58.7360	57.7600	57.7779
105	58.7359	57.7581	57.7747
120	58.7359	57.7567	57.7723
150		57.7553	57.7696
180		57.7546	57.7681
240		57.7543	57.7668
300		57.7543	57.7665
360			57.7665
$W_{30} - W_{\infty}$(grams)	0.0097	0.0336	0.0453
B (grams $min.^{-1}$, sq. cm^{-1})	0.00417	0.00691	0.00750

Casting solution: B-402

Conditions of atmosphere: 24°C; 80 wt.% acetone vapor

Plate Number	10	13	16
Weight of empty plate (grams)	58.7082	57.7194	57.7256
Evaporation period (seconds)	Weight of plate + casting solution (grams)		
15	58.7981	-------	-------
20	-------	57.8497	57.8682
30	58.7876	57.8428	57.8608
45	58.7818	57.8340	57.8513
60	58.7777	57.8269	57.8436
75	58.7751	57.8213	57.8374
90	58.7738	57.8169	57.8323
105	58.7729	57.8133	57.8282
120	58.7726	57.8104	57.8251
150	58.7724	57.8067	57.8208
180	58.7724	57.8045	57.8179
240		57.8028	57.8153
300		57.8026	57.8145
360		57.8026	57.8145
$W_{30} - W_{\infty}$ (grams)	0.0152	0.0402	0.0463
B (grams $min.^{-1}.sq.\ cm^{-1}$)	0.00371	0.00477	0.00517

END OF REEL